Running Title: mEos3.2 photophysics in cells

Optimizing imaging conditions for photoconvertible protein mEos3.2 in live and fixed cells

Mengyuan Sun[1], Kevin Hu[4], Joerg Bewersdorf[3,4*] and Thomas D. Pollard[1,2, 3*]

[1]Departments of Molecular Biophysics and Biochemistry

[2]Departments of Molecular Cellular and Developmental Biology

[3]Department of Cell Biology

[4]Department of Biomedical Engineering

Yale University, PO Box 208103

New Haven, CT 06520-8103 USA

*Correspondence: joerg.bewersdorf@yale.edu; thomas.pollard@yale.edu

Abstract

Photoconvertible fluorescent proteins (PCFPs) are widely used in super-resolution microscopy and studies of cellular dynamics. However, our understanding of their photophysics is still limited, hampering their quantitative application. For example, we do not know the optimal sample preparation methods or imaging conditions to count protein molecules fused to PCFPs by single-molecule localization microscopy in live and fixed cells. We also do not know how the behavior of PCFPs in live cells compares with fixed cells. Therefore, we investigated how formaldehyde fixation influences the photophysical properties of the popular green-to-red PCFP mEos3.2 in fission yeast cells under a wide range of imaging conditions. We estimated photophysical parameters by fitting a 3-state model of photoconversion and photobleaching to the time course of fluorescence signal per yeast cell expressing mEos3.2. We discovered that formaldehyde fixation makes the fluorescence signal, photoconversion rate and photobleaching rate of mEos3.2 sensitive to the buffer conditions by permeabilizing the cell membrane. Under some imaging conditions we tested, the time-integrated mEos3.2 signal per cell is similar in live cells and fixed cells imaged in buffer at pH 8.5 with 1 mM DTT as a reducing agent, indicating that light chemical fixation does not destroy mEos3.2 molecules. We also discovered that 405-nm irradiation converts some mEos3.2 molecules from the green state to an intermediate state that requires 561-nm illumination for conversion to the red fluorescent state. Our findings provide a guide to compare quantitatively and optimize conditions for imaging and counting of mEos3.2-tagged molecules. Our imaging assay and mathematical model are easy to implement and provide a simple quantitative approach to measure the time-integrated signal and the photoconversion and photobleaching rates of fluorescence proteins in cells.

INTRODUCTION

Photoactivatable or photoconvertible fluorescent proteins (PAFPs or PCFPs) have enabled super-resolution imaging by temporally separating closely-spaced molecules (1-3). The fluorescent protein EosFP (4) and its derivatives (5-7) have been widely used in SMLM for both live (8-10) and fixed biological samples (11-13). The fluorescent protein is fused to the coding sequence of a protein of interest in the genome for endogenous expression or expressed exogenously and transiently in cells. Irradiation at 405 nm photoconverts EosFPs from their native green state with an emission peak at 516 nm to their red state with an emission peak at 580 nm (4, 14, 15). Sparsely distributed photoconverted red EosFPs are excited at 561 nm and then localized (13). The rationally designed, monomeric derivative of EosFP mEos3.2 is favored by many due to its monomeric property, high brightness, photostability, and compatibility with live cells (6).

Counting fluorescently-tagged fusion proteins is a potential strength of SMLM, as the images are assembled from discrete localizations of individual molecules (16, 17). The total number of localizations in the SMLM images is closely correlated to the total number of fusion proteins, which allows the measurement of this important quantity even in a diffraction-limited subcellular structure (9, 11, 12, 18-22). Genetically encoded tagging with PAFPs or PCFPs can ensure 1:1 labeling stoichiometry (16), without the uncertainties associated with extrinsic labeling techniques (22-27). However, even with genetically encoded tags, quantitative SMLM still faces several challenges that can lead to undercounting or overcounting the molecules. Fluorescent proteins mature slowly, so an unknown fraction of the FPs is fluorescent at the time of imaging (28). Some of the PAFPs or PCFPs might never be photoconverted or photoactivated to the active state for SMLM imaging (29). Moreover, activated PAFPs or PCFPs may enter a transient dark state and return to the fluorescent state an unknown number of times, which can lead to overcounting (18, 20). A promising way of doing quantitative SMLM is to obtain numbers of the tagged molecules relative to internal calibration standards of known number (9, 11, 12, 21). The sources of error mentioned above can be accounted for if the target and calibration standards are prepared, imaged, and analyzed consistently in the same way (11, 12, 16, 30).

However, any inconsistency in the process of sample preparation, SMLM imaging, or data analysis can introduce errors. Diffusion and other movements of the fluorescent protein can further complicate the quantification process, so light chemical fixation is used to preserve the

targeted structure and eliminate movements for quantitative SMLM of cells expressing proteins tagged with mEos2 (11, 12). However, fixation can introduce measurement errors. For example, fixation might destroy some FPs or change their photophysical properties (31), which can change the average number of localizations for the FP.

In this study, we measured the photophysical properties of mEos3.2 in fission yeast cells by fitting a 3-state model of photoconversion and photobleaching to of the time course the mEos3.2 fluorescence signal per cell measured by quantitative fluorescence microscopy. We found that fixation with formaldehyde permeabilized the cells, making the photophysical properties of mEos3.2 sensitive to the buffer conditions. We imaged fixed cells in buffers with different pH and concentrations of reducing agent DTT to find conditions where the mEos3.2 photophysical parameters are comparable to the live-cell parameters. We tested a wide range of imaging conditions by point-scanning and widefield microscopy to provide guidance for optimizing these conditions for SMLM. We also discovered that 405-nm illumination converts a subpopulation of mEos3.2 molecules to an intermediate state that is photoconverted to the red fluorescent state by 561-nm illumination. Our data provide information to prepare samples for imaging and counting mEos3.2 in live and fixed cells. Our quantitative imaging assay combined with the 3-state model can be applied to study the photophysical properties of other PAFPs and PCFPs quantitatively.

MATERIALS AND METHODS

Plasmids and Strains

The open reading frame encoding mEos3.2 was cloned into the pJK148-pAct1-nmt1Term plasmid with PCR and NEB HiFi Builder Assembly. Both the newly constructed plasmid and chromosomal insertion were verified by sequencing.

Preparation of Cells for Imaging

S. pombe cells expressing mEos3.2 were grown in exponential phase at 25 °C in YE5S-rich liquid medium in 50-mL flasks in the dark before switching to EMM5S-synthetic medium ~12-18 hours before imaging to reduce the cellular autofluorescence background. Live cells were concentrated 10- to 20-fold by centrifugation at 3,000 rpm for 30 s and resuspended in EMM5S for imaging.

Cells were fixed by mixing an equal volume of fresh, room temperature 4% formaldehyde aqueous solution (EMS) with the cell culture and shaking at 150 rpm at 25° C for 15 min or 30 min. The cells were pelleted by centrifugation at 3,000 rpm for 30 s and washed by pelleting in EMM5S or other buffers 3 times, and then resuspended in EMM5S or other buffers. Concentrated cells in 5 µL were mounted on a thin layer formed from 35 µL of 25% gelatin (Sigma-Aldrich; G-2500) in EMM5S or other buffers (without the DTT). To assess how pH and reducing agent affect the photophysical properties of mEos3.2, we fixed cells for 30 min and then washed and resuspended the cells for imaging in one of the following buffers: 50 mM MES (pH 5.5), 50 mM MES (pH 6.5), 50 mM Tris-HCl (pH 7.5), 50 mM Tris-HCl (pH 8.5), 50 mM Tris-HCl (pH 7.5) with 1 mM DTT, 50 mM Tris-HCl (pH 8.5) with 1 mM DTT, or 50 mM Tris-HCl (pH 8.5) with 10 mM DTT.

Point-scanning Confocal Imaging Conditions

Time lapse videos were acquired on a Zeiss Laser Scanning Microscope (LSM 880) using an alphaPlan-Apochromat 100x/NA 1.46 oil-immersion objective and an emission band path filter collecting fluorescence in the 566 - 719 nm wavelength range. Samples were illuminated by scanning a field of view (FOV) of 512 x 512 pixels (1 pixel = 160 nm) with both the 405 nm and 561 nm lasers at constant intensities. To test different imaging conditions, we set the 405 nm laser power at the sample constant ranging from 16 to 56 µW and the 561 nm laser power constant ranging from 11 to 37 µW. To compare with epi-fluorescence imaging conditions, we calculated the average intensity and the peak intensity. The average intensities in the FOV (power at the sample divided by the FOV area) were 0.22 to 0.78 W/cm^2 at 405 nm and 0.15 to 0.51 W/cm^2 at 561 nm. The peak intensities (power at the sample divided by the size of the point spread function) were ~80 to 240 kW/cm^2 at 405 nm and ~20 to 80 kW/cm^2 at 561 nm. A Z-stack of 19 slices spaced at 600-nm intervals was acquired with a pixel dwell time of 0.85 µs. The total exposure time for each Z-stack was 4.23 s (0.85 µs x 512 x 512 x 19). An entire time lapse data set consisted of 50 or 100 Z-stacks that were collected at 15-s intervals including the scan overhead between stacks. For experiments with alternating 405 and 561-nm laser illumination, the 561-nm laser scanned the FOV for 10 cycles followed by 405-nm laser scanning for 5 cycles with either no break or a 2 min break between the 405-nm period and the following 561-nm illumination period. The laser powers at the sample were 56 µW at 405 nm and 37 µW at 561 nm.

For GFP photobleaching measurements, wild type cells and cells expressing Fim1-GFP (TP347) were excited at 488 nm (~60 µW at the sample) and emission fluorescence in the range of 505-735 nm was collected. A 19-slice Z stack with 600-nm intervals covering a FOV of 512 x 512 pixels (1 pixel = 160 nm) was imaged at each time point with a pixel dwell time of 0.85 µs. The entire time-lapse data set consisted of 100 Z-stacks.

Widefield Fluorescence Imaging Conditions

Time lapse videos were acquired with a custom-built single-molecule localization microscope (SMLM) based on a Leica DMi8 stand with epifluorescence illumination, a 63x/1.47 NA oil-immersion objective, and a band pass filter to collect emission fluorescence in the 584-676 nm wavelength range. Samples were illuminated at both 405 nm and 561 nm and imaged with an sCMOS camera (Hamamatsu ORCA-Flash4.0 V2) at 50 frames per second (fps) for 15,000 frames. To test different imaging conditions, the 405-nm laser intensity was set constant ranging from 0.5 to 2 W/cm^2, and the 561-nm laser intensity from 1 W/cm^2 to 1 kW/cm^2.

Image Analysis

Images recorded by confocal and epi-fluorescence microscopes were viewed and analyzed in Fiji (Fiji is Just ImageJ) (32). We made a sum projection of the 19-slice Z-stacks of the time-lapse confocal images. We manually selected a region of interest (ROI) 1 (containing typically ~50-100 cells for the confocal images and ~ 25 cells for the epifluorescence images) with the polygon tool and selected the background ROI 2 with the square tool (Fig. S1). The area and mean signal per pixel (MSPP) of both ROIs were measured and the fluorescence signal per cell at each time point was calculated based on: [Area 1 * (MSPP 1 –MSPP 2)] / number of cells in ROI 1. We calculated the weighted mean and standard deviation of the fluorescence signal per cell from all the FOVs included for each condition, weighted by the number of the cells in each FOV. To correct for autofluorescence background, we subtracted autofluorescence signal per wildtype cell at each time point from the fluorescence signal per cell expressing mEos3.2.

Analytical Model of the Time Course of Red mEos3.2 Fluorescence Signal per Cell

Our three-state model (Fig. 1C) considers mEos3.2 molecules to have 3 different states: a non-activated green (G) state, an activated red (R) state, and a bleached (B) state. Photoconversion converts molecules from the G- to the R-state by an irreversible first order reaction with a rate constant of k_{act} ($k_{activation}$). Molecules in the R-state emit red photons until photobleaching converts them to the B state by an irreversible first-order reaction with a rate constant of k_{bl}

($k_{bleaching}$). With irradiation at 405 nm and 561 nm, the rates of change in the numbers (n) of G-, R-, and B-state mEos3.2 molecules are described by the following differential equations (Fig. S2A):

$$\frac{dG_n}{dt} = -k_{act}G_n \quad (1)$$

$$\frac{dR_n}{dt} = k_{act}G_n - k_{bl}R_n \quad (2)$$

$$\frac{dB_n}{dt} = k_{bl}R_n \quad (3)$$

We defined the total number of mEos3.2 molecules in a cell as M_n, and assumed that all mEos3.2 molecules were in the green state at the start of the experiment, so $G_n(t = 0) = M_n$, $R_n(t = 0) = 0$, and $B_n(t = 0) = 0$. Solving the system of differential equations analytically resulted in the following equations for the number of G-, R-, and B-state molecules in a cell changing over time:

$$G_n(t) = M_n e^{-k_{act}t} \quad (4)$$

$$R_n(t) = \frac{M_n k_{act}}{k_{bl} - k_{act}}\left(e^{-k_{act}t} - e^{-k_{bl}t}\right) \quad (5)$$

$$B_n(t) = \frac{M_n}{k_{bl} - k_{act}}\left[k_{bl}\left(1 - e^{-k_{act}t}\right) - k_{act}\left(1 - e^{-k_{bl}t}\right)\right] \quad (6)$$

Eq. 5 describes how the number of R-state mEos3.2 molecules in a cell (R_n) changes with continuous photoconversion and photobleaching. Assuming that the signal of an R molecule per frame is ε_f, the fluorescence signal from red mEos3.2 molecules per cell (R_s) at each frame recorded at a given time t is $R_s(t) = R_n(t) \times \varepsilon_f$. Multiplying both sides of Eq. 5 by ε_f gives Eq. 7 that describes how the fluorescence signal per cell in each frame $R_s(t)$ changes over time with continuous photoconversion and photobleaching:

$$R_s(t) = \frac{M_n \varepsilon_f k_{act}}{k_{bl} - k_{act}}\left(e^{-k_{act}t} - e^{-k_{bl}t}\right) \quad (7)$$

We estimated $M_n \times \varepsilon_f$, k_{act}, and k_{bl} using Levenberg-Marquardt nonlinear least squares regression to fit Eq. 7 to the time course of fluorescence signal per cell $R_s(t)$. We calculated the 95% confidence intervals of the fitted parameters from the covariance argument of the fit. For the confocal experiments, we fit Eq. 7 to the weighted average time course of fluorescence signal per cell from all FOVs and report the 95% confidence intervals of the fitted parameters. For the epi-fluorescence imaging experiments, we fit Eq. 7 individually to the time course of fluorescence signal per cell (after autofluorescence background subtraction) from each FOV. We

calculated the mean fitted parameters and standard deviation weighted by the number of cells in each FOV.

Since $R_s(t)$ is the fluorescence signal from red mEos3.2 molecules per cell in each frame, the fluorescence signal from red mEos3.2 molecules per cell per second is $R_s(t)$ x f (frame rate, fps). Integrating the function $R_s(t)$ x f with respect to time (t, second) over the interval of [0, ∞] gives the time-integrated signal $\overline{R_s}$ of mEos3.2 per cell:

$$\overline{R_s} = \int_0^\infty [f \cdot R_s(t)]dt = \int_0^\infty \frac{f M_n \varepsilon_f k_{act}}{k_{bl} - k_{act}} (e^{-k_{act}t} - e^{-k_{bl}t})dt = \frac{f M_n}{k_{bl}} \quad (8)$$

We used Eq. 8 to calculate $\overline{R_s}$ using the parameters M_n x ε_f and k_{bl} from the previous fit of Eq. 7. We estimated the 95% CI or standard deviation through error propagation.

Experiments with alternating illumination at 405 nm and 561 nm revealed a fourth intermediate (I) state of mEos3.2 molecules (Fig. 6D). Illumination at 405 nm converts mEos3.2 molecules in the G-state into populations of R-state and I-state molecules. Irradiation at 561 nm converts the mEos3.2 molecules from the I-state to R-state with an activation rate constant of $k_{act,561}$. R-state molecules are photobleached with a bleaching rate constant of k_{bl}. During a 561-nm illumination period after a previous 405-nm illumination period, the rates of change in the numbers (n) of I-, R-, and B-state mEos3.2 molecules are described by the following differential equations:

$$\frac{dI_n}{dt} = -k_{act,561} I_n \quad (9)$$

$$\frac{dR_n}{dt} = k_{act,561} I_n - k_{bl} R_n \quad (10)$$

$$\frac{dB_n}{dt} = k_{bl} R_n \quad (3)$$

We defined the total number of mEos3.2 molecules, i.e. the sum of molecules in the I-, R- and B-states in a cell, after the previous 405-nm irradiation as S_n. We further define t = 0 as the time at which 561-nm illumination starts and assume that S_n is constant during the 561-nm illumination period since the 405-nm laser is shut off and conversion of molecules from the green state by 561-nm light is negligible. We further assume that the number of molecules in the different states at the beginning of the 561-nm illumination period is $R_n(t = 0) = R_{n,0}$, $I_n(t = 0) = S_n - R_{n,0}$, and $B_n(t = 0) = 0$. Solving the system of differential equations analytically resulted in the following equations for the number (n) of I-, R-, B-state molecules changing over time:

$$I_n(t) = (S_n - R_{n,0})e^{-k_{act,561}t} \quad (11)$$

$$R_n(t) = \frac{1}{k_{bl}-k_{act,561}}\left[\left(S_n - R_{n,0}\right)k_{act,561}e^{-k_{act,561}t} - \left(S_n k_{act,561} - R_{n,0}k_{bl}\right)e^{-k_{bl}t}\right] \quad (12)$$

$$B_n(t) = \frac{S_n}{k_{bl}-k_{act,561}}\left[k_{bl}(1-e^{-k_{act,561}t}) - k_{act,561}(1-e^{-k_{bl}t})\right] + \frac{R_{n,0}k_{bl}}{k_{bl}-k_{act,561}}\left(e^{-k_{act,561}t} - e^{k_{bl}t}\right) \quad (13)$$

Eq. 12 describes how the number of red mEos3.2 molecules in a cell (R_n) changes during the period of 561-nm irradiation. Multiplying both sides of Eq. 12 by ε_f gives equation (14) that describes how the fluorescence signal per cell changes over time during this period:

$$R_s(t) = \frac{1}{k_{bl}-k_{act,561}}\left[\left(S_n\varepsilon_f - R_{n,0}\varepsilon_f\right)k_{act,561}e^{-k_{act,561}t} - \left(S_n\varepsilon_f k_{act,561} - R_{n,0}\varepsilon_f k_{bl}\right)e^{-k_{bl}t}\right] \quad (14)$$

We estimated S_n x ε_f, $R_{n,0}$ x ε_f, $k_{act,561}$, and k_{bl} using Levenberg-Marquardt nonlinear least squares regression to fit Eq. 14 to the time courses of the fluorescence signal per cell during the 561-nm illumination period. We calculated the mean and standard deviation of the activation rate constant ($k_{act,561}$) for converting mEos3.2 molecules from I- to R-state by 561-nm irradiation from averaging the 7 periods of 561-nm irradiation for each condition.

Single-molecule Localization

We acquired single R-state mEos3.2 molecules data with our custom-built SMLM using a 405-nm laser intensity of 1 W/cm^2,a 561-nm laser intensity of 1 kW/cm^2, and a frame rate of 50 fps. We localized single molecules with the Python Microscopy Environment (PYME) package (33), using a threshold of 0.6 for event detection computed from the estimated pixel signal-to-noise ratio (SNR).We corrected pixel-dependent noise with maps generated from dark camera frames. We measured the number of photons from single R-state mEos3.2 molecules in each 20-ms frame between frames 5,000 and 10,000 only since the R-state molecules before frame 5,000 were too dense for localization and most were bleached after frame 10,000.

Cell Permeability Experiments

To measure cell permeability, live and fixed wild type cells were prepared as above, and then resuspended in EMM5S medium containing 1 mg/mL fluorescein, fluorescein-dextran 3,000 MW (0.5-1 fluorophores per dextran molecule), fluorescein-dextran 10,000 MW (1-2 fluorophores per dextran molecule), or fluorescein-dextran 70,000 MW (3-8 fluorophores per dextran molecule) from Sigma-Aldrich. The cells were concentrated 10-20 fold by centrifugation at 3,000 rpm for 30 s, and 5 µL of concentrated wild type cells with the fluorescein or

fluorescein-dextran were mounted on a thin layer consisting of 35 µL 25% gelatin (Sigma-Aldrich; G-2500) in EMM5S, sealed under a coverslip with Valap, and imaged at room temperature (~23° C). Bright-field and confocal fluorescence images of the mid-sections of cells were acquired with an Olympus IX-71 microscope with a 100x/NA1.4 Plan Apo lens (Olympus) and a CSU-X1 (Andor Technology) confocal spinning-disk system with an IXON-EMCCD camera (Andor Technology).

RESULTS

Quantitative assessment of mEos3.2 photophysics *in vivo* by fitting our 3-state model to quantitative fluorescent microscopy data

We combined quantitative fluorescence microscopy with mathematical modeling to estimate the time-integrated signal per cell ($\overline{R_s}$), and the rate constants for photoconversion and photobleaching (k_{act} and k_{bl}) of mEos3.2 in the cytoplasm of fission yeast cells (Fig. 1). Our model assumes that illumination at 405 nm photoconverts mEos3.2 molecules irreversibly from their green (G) to their red (R) state with an activation rate constant of k_{act} and that the 561-nm light excites the red-form mEos3.2 with a peak emission at ~580 nm. Irradiation at either 405 nm or 561 nm converts R-state mEos3.2 molecules to the bleached (B) state by an irreversible first-order reaction with a bleaching rate constant of k_{bl} (Fig. 1C).

Fission yeast cells expressing mEos3.2 from the actin promoter in the *leu1* locus ensured a relatively high and homogenous cytoplasmic mEos3.2 expression level (Fig. 1A). We used point-scanning confocal microscopy to illuminate the cells at both 405 nm and 561 nm and collect time-lapse images in the red wavelength range of 566-719 nm (Fig. 1A). The time course of fluorescence signal per cell first rose as the large pool of molecules in the G-state was photoconverted to the R-state, from which we detected red photons as signal, and then declined as the pool of molecules in the G-state was depleted and photobleaching depleted the R-state pool (Fig. 1B).

The equation (Eq. 7) of our 3-state model (Fig. 1C) fit the time courses of fluorescence signal per cell very closely (Fig. 1B). The best fits yielded estimates of the product of total number of molecules per cell and detected signal per R-state molecule per frame (M_n x ε_f), and the rate constants for photoconversion (k_{act}) and photobleaching (k_{bl}) (Table S1). We then used Eq. 8 to calculate the time-integrated signal per cell ($\overline{R_s}$) using fitted parameters M_n x ε_f and k_{bl}

(Table S1). We used this approach to measure how sample preparation and imaging conditions influence these photophysical properties.

Effects of formaldehyde fixation and imaging buffer on photophysical properties of mEos3.2

We investigated how fixation affects the photophysical properties of mEos3.2, so we could compare experiments on live and fixed cells (Fig. 2). Cells fixed with formaldehyde in EMM5S-synthetic growth medium emitted fewer red photons than live cells imaged under the same conditions (Fig. 2C). Fitting Eq. 7 of the 3-state model (Fig. 1C) to the time courses of fluorescence signal per cell showed that fixation reduced $M_n \times \varepsilon_f$ (Fig. 2D) and $\overline{R_s}$ (Fig. 2G) and increased k_{act} (Fig. 2E) and k_{bl} (Fig. 2F). Longer fixation further decreased the fluorescence signals (Fig. 2D, G) and increased both rate constants (Fig. 2E, F).

We used fluorescein-dextrans to test our hypothesis that formaldehyde fixation changes mEos3.2 photophysics by permeabilizing the cell membrane (Fig. S3). Live yeast cells excluded fluorescein and all fluorescein-dextrans that we tested, but fixation with formaldehyde (without detergents or organic solvents) permeabilized the cell membrane, allowing the entry of fluorescein-dextrans up to 10,000 MW (Fig. S3). Thus, ions and small molecules in the buffer used for imaging fixed cells equilibrated with the interior of the fixed cells and affected the photophysical properties of mEos3.2.

Knowing that fixed cells are permeable, we tested how the composition of the imaging buffer influenced mEos3.2 photophysics (Fig. 3). We hypothesized that the photophysical changes of mEos3.2 in the fixed cells were due to the low pH (~5.5) and oxidizing environment of EMM5S relative to the live-cell cytoplasmic environment. We found that $\overline{R_s}$ was higher (Fig. 3B), and k_{act} (Fig. 3D) and k_{bl} (Fig. 3E) were lower in imaging buffers with higher pH. Adding the reducing agent DTT to the imaging buffer further increased $\overline{R_s}$ (Fig. 3B) and decreased k_{bl} in the pH range we tested (Fig. 3E). A concentration of 1 mM DTT was more effective than 10 mM DTT at increasing $\overline{R_s}$ (Fig. 3B). Additionally, the value of $M_n \times \varepsilon_f$ from fixed cells in 50 mM Tris-HCl (pH 8.5) with 1 mM DTT (9187 A.U., 95% CI: 9024 – 9351, Table S2) was similar to that from live cells (9489 A.U., 95% CI: 9291 - 9687, Table S1). Values of $\overline{R_s}$ were also similar in live cells and fixed cells at pH 8.5 with 1 mM DTT (Table S1, S2). Thus, mEos3.2 molecules survived fixation and the total number of fluorescence-competent molecules per cell (M_n) did not

change, but the extracellular imaging buffer influenced the intracellular mEos3.2 signal per frame (ε_f) and other photophysical properties as photoconversion and photobleaching rates.

Effects of the 405-nm and 561-nm laser intensities on photophysical properties of mEos3.2

We used laser-scanning confocal microscopy and epi-fluorescence microscopy to test the effects of a wide range of laser intensities on mEos3.2 photophysics in fixed cells in imaging buffer at pH 8.5 with 1 mM DTT (Fig. 4). The product of total mEos3.2 molecules per cell and signal of R-state molecule per frame ($M_n \times \varepsilon_f$) were similar in live cells and fixed cells in the imaging buffer of pH 8.5 with 1 mM DTT (Fig. 4A-D), including the SMLM imaging conditions with a 405-nm laser intensity of 0.5-2 W/cm^2 and a 561-nm laser intensity of 1 kW/cm^2 (Fig. 4C). However, the time-integrated signal per cell ($\overline{R_s}$) differed in live cells and fixed cells in the alkaline imaging buffer with DTT at 561-nm laser intensities of 10 and 100 W/cm^2 (Fig. 4P).

To optimize imaging conditions quantitatively, we explored the effects of laser intensities on mEos3.2 photophysics by point-scanning illumination (Fig. 4, left 2 columns). $\overline{R_s}$ decreased (Fig. 4M), and both rate constants (Fig. 4E, I) increased with higher 405-nm laser intensity. $\overline{R_s}$ increased with higher 561-nm laser intensity (Fig. 4N), but 561-nm laser intensity had only modest effects on both rate constants (Fig. 4F, J) in the range we tested.

We used widefield illumination to explore the effects of a wider range of 561-nm laser intensities on mEos3.2 photophysics, including the high 561-nm laser intensity of ~1 kW/cm^2 used in SMLM (Fig. 4, right 2 columns). Values of k_{bl} increased with higher 405-nm laser intensity (Fig. 4K), as observed with point-scanning illumination (Fig. 4I), but the 405-nm laser intensity had remarkably little impact on the k_{act} (Fig. 4G) and $\overline{R_s}$ (Fig. 4O) under SMLM conditions. $\overline{R_s}$ increased with higher 561-nm laser intensity and then plateaued and dropped (Fig. 4P). Interestingly, the 561-nm laser intensity at the maximum $\overline{R_s}$ differed in live cell and fixed cell in different buffers (Fig. 4P). Both k_{act} and k_{bl} increased dramatically with 561-nm laser intensities (Fig. 4H, L), which was not seen with a much narrower range of low 561-nm laser intensities by point-scanning illumination (Fig. 4F, J).

Photon counts from single red-state mEos3.2 molecules in live and fixed cells

To assess the effects of fixation and the imaging buffer on mEos3.2 photophysics under SMLM conditions, we compared the photon counts of single R-state mEos3.2 molecules per frame in

live and fixed yeast cells (Fig. 5). Under SMLM imaging conditions with a frame rate of 50 fps and a 561-nm laser intensity of 1 kW/cm^2, R-state mEos3.2 molecules were sparse enough to be localized after photobleaching a large fraction of mEos3.2 molecules. We localized single molecules in each frame and measured their photon counts in each frame.

Fixation decreased the mean photon counts from single R-state molecules in each frame, while the values were similar in live and fixed cells imaged in the buffer at pH 8.5 with 1 mM DTT (Fig. 5). Therefore, using the alkaline imaging buffer with DTT instead of EMM5S for imaging mEos3.2 in fixed cells can increase the signal-to-noise ratio of single molecules per frame, thus improving localization precision (34). Combining with the measurements showing that fixation slightly increased $\overline{R_s}$ (Fig. 4O, Table S4), our data suggested that fixation prolonged the duration that mEos3.2 molecules are in the red fluorescent state.

Illumination at 405 nm converts a subpopulation of mEos3.2 molecules to an intermediate state that requires 561-nm irradiation to reach the red fluorescent state

Conversion of G-state mEos3.2 to R-state is usually assumed to be a single irreversible reaction driven by 405-nm irradiation alone (14) (Fig. 1C). Applying alternating periods of multiple cycles of 405-nm and 561-nm irradiation showed, however, that illumination at 561 nm led to an increase of the red mEos3.2 fluorescence signal after a previous period of 405-nm illumination (Fig. 6A). During each period of 561-nm illumination (except for the first one preceding the first 405-nm illumination period), the signal rose transiently above the initial value despite the 405-nm illumination being switched off. After peaking during the second cycle of each 561 nm illumination period, the signal decreased due to photobleaching (Fig. 6A, B). The signal during each 561-nm illumination period (except for the first one) followed similar time courses for the duration of these experiments (Fig. 6B).

We considered four hypotheses to explain these transient increases in the fluorescence signal. First, illumination at 561 nm might photoconvert G-state mEos3.2 to the R-state directly, but we observed no comparable activation with 561-nm irradiation alone (Fig. 6C, and first ten cycles of 561-nm irradiation in Fig. 6A). A second hypothesis is that the first-order photoconversion reaction is slow after absorption of 405-nm photons, delaying accumulation of R-state molecules. We ruled out this mechanism with a modified experiment adding a 2-min pause after each 405-nm illumination period and before the onset of the following 561-nm

illumination period. The transient increase in the fluorescence signal was still observed, ruling out this hypothesis as a dominating effect (Fig. 6A, B). Similarly, we could rule out the third hypothesis that the observed increase in the fluorescence signal over the course of 561-nm illumination was related to protein maturation or similar live-cell phenomena by observing the same effect in fixed cells (Fig. S7A, B).

The fourth hypothesis is that 405-nm illumination converts a subpopulation of G-state mEos3.2 molecules to an intermediate (I) state that requires 561-nm illumination to reach the R-state. To test this hypothesis, we added a fourth I-state to the model (Fig. 6D). Eq. 14 of our 4-state model fit closely the time courses of mEos3.2 fluorescence signal during each 561-nm illumination period (Fig. 6B). The best fits gave an average activation rate constant ($k_{act,561}$) of 0.27 s^{-1} (SD: 0.03 s^{-1}) from I-state to R-state by 561-nm irradiation (Fig. 6B), which is 4-fold higher than in the G- to R-state photoconversion rate constant (k_{act}) of 0.050 s^{-1} (95% CI: 0.048-0.051 s^{-1}) as measured with simultaneous 405-nm and 561-nm illumination (Fig. S7C).

These experiments revealed that 405-nm irradiation converts G-state mEos3.2 molecules to either R-state or I-state, and 561-nm irradiation is required to convert the I-state molecules to the R-state (Fig. 6D). However, for experiments with simultaneous illumination at both 405 nm and 561 nm, Eq. 7 of our 3-state model fully accounted for the time courses of fluorescence signal per cell under all the conditions (Fig. 1B, 2C, 3A, S5, S6).

DISCUSSION

Characterizing the photophysics of mEos3.2 by fitting our 3-state model to quantitative time-lapse fluorescence microscopy data

We show how to measure the product of total number of molecules per cell and the signal of R-state molecule per frame (M_n x ε_f) and rate constants for photoconversion (k_{act}) and photobleaching (k_{bl}) in cells by fitting a simple 3-state model to the time course of measured fluorescence signals (Fig. 1). Eq. 7 of our 3-state model fit the time courses of the fluorescence signal per cell very closely (Fig. 2C, 3A) and revealed how different conditions changed the three parameters separately. Furthermore, simulations of the 3-state model showed how the values of the three parameters influenced the time courses of the number of R-state molecules per cell (Fig. S2B – D). We also used Eq. 8 to calculate the time-integrated signal per cell ($\overline{R_s}$) using M_n x ε_f and k_{bl}.

Our approach has several advantages over the alternative approach characterizing single fluorescent molecules *in vitro* (18, 35, 36). Our approach is easy to implement in cells, as it does not require setting thresholds for single-molecule detection and fitting with the high background in cells. Moreover, our approach can extract photoconversion or photoactivation rate constants in cells, which is useful for optimizing SMLM imaging conditions and simulating more realistic SMLM raw data. Extracting these rate constants from the single-molecule data from only one channel is challenging as the effect of photobleaching cannot be accounted for (29). The limitation of our approach is that we cannot measure the single-molecule blinking kinetics of the fluorophores. Combining our approach with single-molecule characterization of fluorescent proteins, which provides access to the blinking kinetics, will offer a complete and quantitative understanding of the photophysics of PAFPs or PCFPs for SMLM application.

Optimizing sample preparation for imaging mEos3.2 in fixed fission yeast cells

Preserving the fluorescence signal and structures of interest is crucial when fixing cells with fluorescent protein labels. We showed that formaldehyde fixation did not destroy mEos3.2 molecules but permeabilized yeast cells, so the photophysical properties of mEos3.2 were sensitive to the composition of the imaging buffer. The low pH of 5.5 and lack of oxygen scavenging system in the EMM5S synthetic medium affected the photophysical properties of mEos3.2 in fixed cells as expected from previous works showing that EosFP photoconverts faster (4) and mEos3.2 emits fewer red photons at acidic pH (6). Photooxidation can increase the photobleaching rate (37). Oxygen in the solution can also affect the fluorescence signal by promoting intersystem crossing (38) and convert the excited molecules to the non-fluorescent triplet state.

Our experiments also show that fixation conditions must be tested and optimized for each fluorescent protein. For example, longer duration of fixation with formaldehyde further reduced $\overline{R_s}$ and increased k_{act} and k_{bl} of mEos3.2 under the imaging condition we tested (Fig. 2E-G). On the other hand, GFP was far less sensitive to fixation, as formaldehyde treatment had little effect on its fluorescence signal and photobleaching rate (Fig. S8).

On the other hand, using an imaging buffer with alkaline pH and reducing agent modulated the mEos3.2 photophysics in fixed cells (Fig. 3). Imaging buffers with a pH equal to or slightly higher than the cytoplasmic pH of fission yeast at ~7.3 (39) increased $\overline{R_s}$ and reduced

k_{act} and k_{bl} (Fig. 3B, D, E). Adding a reducing agent to the imaging buffer further increased $\overline{R_s}$ (Fig. 3B). An imaging buffer at pH 8.5 with 1 mM DTT not only maintained the photon counts of single R-state mEos3.2 molecules in each frame (Fig. 5) but also reduced the cellular autofluorescence compared to imaging fixed cells in EMM5S medium (Fig. 2B, S4B). This is crucial for SMLM imaging, where the signal-to-noise ratio is important for obtaining high localization precision and consequently resolution (34).

Comparison of point-scanning and widefield illumination for mEos3.2 photophysics

We compared the photophysical properties of mEos3.2 when illuminated by point-scanning and widefield microscopy. Under point-scanning illumination, each area of the sample was illuminated for a very short time at high peak intensity (e.g. ~80 kW/cm^2, Fig. 4), while the other pixels were kept in the dark. Thus, the average intensity of the laser power over the entire field of view was ~10^4 times lower than the peak intensity (e.g. ~0.5 W/cm^2, Fig. 4).

Despite huge differences in the instantaneous peak intensities in point-scanning and widefield microscopy, the rate constants for photoconversion and photobleaching in live cells were similar at comparable average intensities (Table S3, S4). For example, with average intensities of ~ 0.5 to 1.1 W/cm^2 for both lasers, confocal and widefield imaging of live cells gave similar k_{act} (~1.5 x 10^{-2} s^{-1} vs. ~5 x 10^{-2} s^{-1}) and k_{bl} (~2 x 10^{-3} s^{-1} vs. ~1 x 10^{-3} s^{-1}). Moreover, the photophysical parameters of mEos3.2 trended similarly with illumination intensities by both point-scanning confocal and widefield microscopy. For example, k_{bl} increased with higher 405-nm intensity (Fig. 4I, K) and M_n x ε_f increased with higher 561-nm laser intensity (Fig. 4B, D). These trends diverged (Fig. 4F, H, J, L) at higher 561-nm laser intensities of 100 and 1000 W/cm^2 outside the range of the confocal microscope.

The effects of the buffer and sample preparation on mEos3.2 photophysics depended on the intensity of 561-nm irradiation, but not the illumination method. For example, $\overline{R_s}$ was lower in cells fixed in EMM5S (pH 5.5) than live cells under low 561-nm laser intensity at 1-10 W/cm^2 (Fig. 4N), while $\overline{R_s}$ from cells fixed in EMM5S was higher than live cells under high 561-nm laser intensity at 1 kW/cm^2 (Fig. 4P). Imaging fixed cells in buffer at pH 8.5 with 1 mM DTT increased $\overline{R_s}$ only under low 561-nm laser intensity of 1-10 W/cm^2 (Fig. 4P). Since the fluorescence signal of red mEos3.2 is lower at acidic pH independent of 561-nm intensity (6), we suspected the different effects of fixation and buffer on mEos3.2 photophysics depending on the

561-nm laser intensity (Fig. 4P) were due to oxidation rather than pH. Thus, the actual conditions should be tested to ensure the oxygen scavenger systems work for one's experiment.

Optimizing laser intensities for imaging mEos3.2 in live and fixed fission yeast cells

Our quantitative measurements provide guidance for selecting laser intensities to image proteins tagged with mEos3.2. Maximizing the red fluorescence signal of mEos3.2 while maintaining a relatively low level of autofluorescence background is the key to optimize imaging quality. Higher signal-noise-ratios can increase localization precision and thus the resolution in SMLM (34). For SMLM, it is crucial to control the density of active fluorophores, so that they are sparse enough for localization but also dense enough to image quickly. The density of active fluorophores can be regulated by changing the rates of photoconversion and photobleaching. High laser intensities are usually used for fast SMLM imaging in fixed samples (35).

Higher 405-nm illumination intensity had four effects on SMLM image quality: (1) it decreased $\overline{R_s}$ under low average 561-nm laser intensity of ~ 0.3 W/cm^2 (Fig. 4M), but the effect was not obvious under high 561-nm laser intensity of 1 kW/cm^2 (Fig. 4O); (2) it increased background autofluorescence (Fig. S5B, E, H), especially in live cells (Fig. S5B); (3) it increased k_{act} (Fig. 4E); and (4) it increased k_{bl} (Fig. 4I, K). One may ramp up 405-nm laser intensity while imaging a field of view to increase k_{act} and compensate for the loss of bleached molecules. However, high 405-nm laser intensities can potentially decrease SMLM imaging quality in two ways: increasing autofluorescence can compromised accurate localization; and rapid photobleaching decreases $\overline{R_s}$, potentially decreasing total number of localizations.

The time-integrated signal $\overline{R_s}$ increased with 561-nm laser intensity (Fig. 4N), reached a maximum and decreased (Fig. 4P) with the peaks for live and fixed cells at different 561-nm laser intensities. The 561-nm laser intensity had less impact on $\overline{R_s}$ from fixed cells in the imaging buffer at pH 8.5 with 1 mM DTT than live cells and fixed cells in EMM5S. Therefore, imaging fixed cells in the alkaline imaging buffer with DTT will be faster with higher 561-nm laser intensity, while the imaging quality is maintained as $\overline{R_s}$ will be largely unchanged. For time-lapse imaging of dynamics in live cells, low 561-nm laser intensity can avoid rapid photobleaching and a huge decrease in $\overline{R_s}$, which can avoid reducing the total number of localizations and tracking times of molecules of interest. The photoconversion (Fig. 4H) and photobleaching rates (Fig. 4L) also increased at high 561-nm laser intensities. The photoconversion rate increases

likely because 561-nm illumination converts mEos3.2 molecules in the intermediate state to the red fluorescent state (Fig. 6D). Thus, one might need to use a lower 405-nm laser intensity to achieve an optimal molecule density when using a higher 561-nm laser intensity.

Application of our findings to quantitative SMLM with mEos3.2 in live and fixed cells

Several variants of EosFP fluorescent proteins are widely used in quantitative SMLM for imaging and counting molecules in both live and fixed cells (9, 11, 12). The time-integrated signal ($\overline{R_s}$) determines the number of mEos3.2 localizations that can be detected in biological samples. The single-molecule brightness also affects the number of mEos3.2 localizations detected, as only the molecules emitting more than a threshold number of photons at each frame will be detected and localized (33). Under SMLM imaging conditions (Fig. 4O), $\overline{R_s}$ was different in live cells and fixed cells in the imaging buffer at pH 8.5 with 1 mM DTT, making direct comparison of the measurements on calibration standards tagged with mEos3.2 molecules in live cells and fixed cell problematic. However, the photon counts from single mEos3.2 emission bursts at each frame by SMLM were similar in live cells and fixed cells (Fig. 5), making it possible to use the same analysis thresholds for single-molecule localization. Our data also suggested that the number of frames when each mEos3.2 molecule is in the R-state is lower in the fixed cells in the imaging buffer at pH 8.5 with 1 mM DTT than live cells, which can be useful to avoid overcounting problems caused by blinking. Baldering *et al.* also showed that the reducing agent BME decreased the number of blinking cycles of mEos3.2 (40).

Illumination at 561-nm is required for mEos3.2 to reach the red fluorescent state from the intermediate state

Our alternating illumination experiments (Fig. 6) revealed that 405-nm irradiation converts mEos3.2 molecules to two different states: the red fluorescent (R) state; and an intermediate (I) state that requires 561-nm irradiation to convert to the R-state. We do not know if the intermediate state is a transient dark state or can be excited at other wavelengths.

Other fluorescent proteins have been reported to undergo two-step photoactivation or photoconversion. We previously reported that a subfraction of PA-mCherry molecules required a similar two-step photoactivation process by both the activation and the excitation lasers (41). Near-ultraviolet activation initially decarboxylates the Glu-215 residue of PA-mCherry resulting

in the oxidation of Try-67 C^{α}-C^{β} and deprotonation of the chromophore. Illumination by the 568-nm excitation laser switches the chromophore between the *cis* and *trans* configurations of the double bond between the C^{α} atom of Try-67 and imidazolone ring (42). Only the decarboxylated and deprotonated *trans* form is fluorescent. De Zitter *et al.* also reported that mEos4b – an mEos3.2 derivative - recovered from the long-lived dark state to the red state in response to 561-nm illumination (43). The long-lived dark state recovery rate increased with higher 561-nm laser intensity. Our work showed that the photoconversion rate (k_{act}) of mEos3.2 from the G- to the R- state increased with higher 561-nm laser intensity (Fig. 4H). Therefore, the I-state we observed for mEos3.2 could be a long-lived dark state as described for mEos4b.

CONCLUSION

In this work, we measured the time-integrated signal per cell, photoconversion and photobleaching rate constants of photoconvertible fluorescent protein mEos3.2 in fission yeast cells by fitting a 3-state model to time-lapse quantitative fluorescence microscopy data. We found that formaldehyde fixation affected mEos3.2 photophysics by permeabilizing the cell membrane and equilibrating the intracellular environment with the imaging buffer. Reducing agent and pH of the imaging buffer affected mEos3.2 photophysics in fixed cells. Using an imaging buffer at pH 8.5 with 1 mM DTT gave a time-integrated signal comparable to live cells under certain imaging condition, suggesting that mEos3.2 molecules survived the light chemical fixation. We tested a wide range of laser intensities by point-scanning and widefield microscopy to provide guidance for optimizing image quality and counting. We discovered an intermediate state of mEos3.2 created by 405-nm illumination that requires 561-nm illumination to convert to the red fluorescent state. Our results provide guidance for sample preparation and laser intensities for imaging and counting mEos3.2-tagged molecules in cells. Our imaging assay and 3-state model can also be applied to study the photophysical properties of other photoactivatable or photoconvertible fluorescent proteins.

SUPPORTING MATERIAL

Supporting Material can be found online at ***.

AUTHOR CONTRIBUTIONS

HS, JB and TDP designed research; HS carried out the experiments; KH built the single-molecule localization microscope and assisted in imaging and data analysis; all authors analyzed the data and wrote the paper.

ACKNOWLEDGMENTS

Research reported in this publication was supported by National Institute of General Medical Sciences of the National Institutes of Health under award number R01GM026132 and R01 GM118486, and the Wellcome Trust (203285/B/16/Z). MS and KH were supported by NIH Grant No. T32EB019941. The content is solely the responsibility of the authors and does not necessarily represent the official views of the National Institutes of Health. The authors thank Bennett Rollins and Zach Marin for help with single-molecule localization imaging and data analysis, and Yongdeng Zhang for helpful discussion. We also acknowledge support from the Program in Physics, Engineering and Biology.

References:

1. Rust, M. J., M. Bates, and X. Zhuang. 2006. Sub-diffraction-limit imaging by stochastic optical reconstruction microscopy (STORM). Nat Methods 3:793-795.
2. Betzig, E., G. H. Patterson, R. Sougrat, O. W. Lindwasser, S. Olenych, J. S. Bonifacino, M. W. Davidson, J. Lippincott-Schwartz, and H. F. Hess. 2006. Imaging intracellular fluorescent proteins at nanometer resolution. Science 313:1642-1645.
3. Hess, S. T., T. P. K. Girirajan, and M. D. Mason. 2006. Ultra-high resolution imaging by fluorescence photoactivation localization microscopy. Biophysical Journal 91:4258-4272.
4. Wiedenmann, J., S. Ivanchenko, F. Oswald, F. Schmitt, C. Rocker, A. Salih, K. D. Spindler, and G. U. Nienhaus. 2004. EosFP, a fluorescent marker protein with UV-inducible green-to-red fluorescence conversion. Proc Natl Acad Sci U S A 101:15905-15910.
5. McKinney, S. A., C. S. Murphy, K. L. Hazelwood, M. W. Davidson, and L. L. Looger. 2009. A bright and photostable photoconvertible fluorescent protein. Nat Methods 6:131-133.
6. Zhang, M., H. Chang, Y. Zhang, J. Yu, L. Wu, W. Ji, J. Chen, B. Liu, J. Lu, Y. Liu, J. Zhang, P. Xu, and T. Xu. 2012. Rational design of true monomeric and bright photoactivatable fluorescent proteins. Nat Methods 9:727-729.
7. Paez-Segala, M. G., M. G. Sun, G. Shtengel, S. Viswanathan, M. A. Baird, J. J. Macklin, R. Patel, J. R. Allen, E. S. Howe, G. Piszczek, H. F. Hess, M. W. Davidson, Y. Wang, and L. L. Looger. 2015. Fixation-resistant photoactivatable fluorescent proteins for CLEM. Nat Methods 12:215-218, 214 p following 218.

8. Laplante, C., F. Huang, I. R. Tebbs, J. Bewersdorf, and T. D. Pollard. 2016. Molecular organization of cytokinesis nodes and contractile rings by super-resolution fluorescence microscopy of live fission yeast. Proc Natl Acad Sci U S A.
9. Zhang, Y., M. Lara-Tejero, J. Bewersdorf, and J. E. Galan. 2017. Visualization and characterization of individual type III protein secretion machines in live bacteria. Proc Natl Acad Sci U S A 114:6098-6103.
10. Akamatsu, M., Y. Lin, J. Bewersdorf, and T. D. Pollard. 2017. Analysis of interphase node proteins in fission yeast by quantitative and superresolution fluorescence microscopy. Mol Biol Cell 28:3203-3214.
11. Puchner, E. M., J. M. Walter, R. Kasper, B. Huang, and W. A. Lim. 2013. Counting molecules in single organelles with superresolution microscopy allows tracking of the endosome maturation trajectory. Proc Natl Acad Sci U S A 110:16015-16020.
12. Fricke, F., J. Beaudouin, R. Eils, and M. Heilemann. 2015. One, two or three? Probing the stoichiometry of membrane proteins by single-molecule localization microscopy. Sci Rep 5:14072.
13. Shroff, H., C. G. Galbraith, J. A. Galbraith, H. White, J. Gillette, S. Olenych, M. W. Davidson, and E. Betzig. 2007. Dual-color superresolution imaging of genetically expressed probes within individual adhesion complexes. P Natl Acad Sci USA 104:20308-20313.
14. Nienhaus, K., G. U. Nienhaus, J. Wiedenmann, and H. Nar. 2005. Structural basis for photo-induced protein cleavage and green-to-red conversion of fluorescent protein EosFP. Proc Natl Acad Sci U S A 102:9156-9159.
15. Turkowyd, B., A. Balinovic, D. Virant, H. G. G. Carnero, F. Caldana, M. Endesfelder, D. Bourgeois, and U. Endesfelder. 2017. A General Mechanism of Photoconversion of Green-to-Red Fluorescent Proteins Based on Blue and Infrared Light Reduces Phototoxicity in Live-Cell Single-Molecule Imaging. Angew Chem Int Edit 56:11634-11639.
16. Coffman, V. C., and J. Q. Wu. 2012. Counting protein molecules using quantitative fluorescence microscopy. Trends Biochem Sci 37:499-506.
17. Baddeley, D., and J. Bewersdorf. 2017. Biological Insight from Super-Resolution Microscopy: What We Can Learn from Localization-Based Images. Annu Rev Biochem.
18. Lee, S. H., J. Y. Shin, A. Lee, and C. Bustamante. 2012. Counting single photoactivatable fluorescent molecules by photoactivated localization microscopy (PALM). Proc Natl Acad Sci U S A 109:17436-17441.
19. Rollins, G. C., J. Y. Shin, C. Bustamante, and S. Presse. 2015. Stochastic approach to the molecular counting problem in superresolution microscopy. Proc Natl Acad Sci U S A 112:E110-118.
20. Annibale, P., S. Vanni, M. Scarselli, U. Rothlisberger, and A. Radenovic. 2011. Quantitative photo activated localization microscopy: unraveling the effects of photoblinking. PLoS One 6:e22678.
21. Hummer, G., F. Fricke, and M. Heilemann. 2016. Model-independent counting of molecules in single-molecule localization microscopy. Mol Biol Cell 27:3637-3644.
22. Ehmann, N., S. van de Linde, A. Alon, D. Ljaschenko, X. Z. Keung, T. Holm, A. Rings, A. DiAntonio, S. Hallermann, U. Ashery, M. Heckmann, M. Sauer, and R. J. Kittel. 2014. Quantitative super-resolution imaging of Bruchpilot distinguishes active zone states. Nat Commun 5:4650.

23. Virant, D., B. Traenkle, J. Maier, P. D. Kaiser, M. Bodenhofer, C. Schmees, I. Vojnovic, B. Pisak-Lukats, U. Endesfelder, and U. Rothbauer. 2018. A peptide tag-specific nanobody enables high-quality labeling for dSTORM imaging. Nat Commun 9:930.
24. Gautier, A., A. Juillerat, C. Heinis, I. R. Correa, Jr., M. Kindermann, F. Beaufils, and K. Johnsson. 2008. An engineered protein tag for multiprotein labeling in living cells. Chem Biol 15:128-136.
25. Los, G., A. Darzins, N. Karassina, C. Zimprich, R. Learish, M. McDougall, L. Encell, R. Friedman-Ohana, M. Wood, and G. Vidugiris. 2005. HaloTag™ Interchangeable labeling technology for cell imaging and protein capture. Cell Notes 11:2-6.
26. Jungmann, R., M. S. Avendano, M. Dai, J. B. Woehrstein, S. S. Agasti, Z. Feiger, A. Rodal, and P. Yin. 2016. Quantitative super-resolution imaging with qPAINT. Nat Methods 13:439-442.
27. Thevathasan, J. V., M. Kahnwald, K. Cieslinski, P. Hoess, S. K. Peneti, M. Reitberger, D. Heid, K. C. Kasuba, S. J. Hoerner, Y. Li, Y. L. Wu, M. Mund, U. Matti, P. M. Pereira, R. Henriques, B. Nijmeijer, M. Kueblbeck, V. J. Sabinina, J. Ellenberg, and J. Ries. 2019. Nuclear pores as versatile reference standards for quantitative superresolution microscopy. Nat Methods 16:1045-1053.
28. Wang, S., J. R. Moffitt, G. T. Dempsey, X. S. Xie, and X. Zhuang. 2014. Characterization and development of photoactivatable fluorescent proteins for single-molecule-based superresolution imaging. Proc Natl Acad Sci U S A 111:8452-8457.
29. Durisic, N., L. Laparra-Cuervo, A. Sandoval-Alvarez, J. S. Borbely, and M. Lakadamyali. 2014. Single-molecule evaluation of fluorescent protein photoactivation efficiency using an in vivo nanotemplate. Nat Methods 11:156-162.
30. Wu, J. Q., and T. D. Pollard. 2005. Counting cytokinesis proteins globally and locally in fission yeast. Science 310:310-314.
31. Ganguly, S., A. H. Clayton, and A. Chattopadhyay. 2011. Fixation alters fluorescence lifetime and anisotropy of cells expressing EYFP-tagged serotonin1A receptor. Biochem Biophys Res Commun 405:234-237.
32. Schindelin, J., I. Arganda-Carreras, E. Frise, V. Kaynig, M. Longair, T. Pietzsch, S. Preibisch, C. Rueden, S. Saalfeld, B. Schmid, J. Y. Tinevez, D. J. White, V. Hartenstein, K. Eliceiri, P. Tomancak, and A. Cardona. 2012. Fiji: an open-source platform for biological-image analysis. Nat Methods 9:676-682.
33. Lin, R., A. H. Clowsley, I. D. Jayasinghe, D. Baddeley, and C. Soeller. 2017. Algorithmic corrections for localization microscopy with sCMOS cameras - characterisation of a computationally efficient localization approach. Opt Express 25:11701-11716.
34. Deschout, H., F. Cella Zanacchi, M. Mlodzianoski, A. Diaspro, J. Bewersdorf, S. T. Hess, and K. Braeckmans. 2014. Precisely and accurately localizing single emitters in fluorescence microscopy. Nat Methods 11:253-266.
35. Lin, Y., J. J. Long, F. Huang, W. C. Duim, S. Kirschbaum, Y. Zhang, L. K. Schroeder, A. A. Rebane, M. G. Velasco, A. Virrueta, D. W. Moonan, J. Jiao, S. Y. Hernandez, Y. Zhang, and J. Bewersdorf. 2015. Quantifying and optimizing single-molecule switching nanoscopy at high speeds. PLoS One 10:e0128135.
36. Zanacchi, F. C., C. Manzo, A. S. Alvarez, N. D. Derr, M. F. Garcia-Parajo, and M. Lakadamyali. 2017. A DNA origami platform for quantifying protein copy number in super-resolution. Nat Methods 14:789-792.

37. Greenbaum, L., C. Rothmann, R. Lavie, and Z. Malik. 2000. Green fluorescent protein photobleaching: a model for protein damage by endogenous and exogenous singlet oxygen. Biological chemistry 381:1251-1258.
38. Mclean, A. J., D. J. Mcgarvey, T. G. Truscott, C. R. Lambert, and E. J. Land. 1990. Effect of Oxygen-Enhanced Intersystem Crossing on the Observed Efficiency of Formation of Singlet Oxygen. J Chem Soc Faraday T 86:3075-3080.
39. Zhang, Y., H. Shen, H. Liu, H. Feng, Y. Liu, X. Zhu, and X. Liu. 2017. Arp2/3 complex controls T cell homeostasis by maintaining surface TCR levels via regulating TCR(+) endosome trafficking. Sci Rep 7:8952.
40. Baldering, T. N., M. S. Dietz, K. Gatterdam, C. Karathanasis, R. Wieneke, R. Tampe, and M. Heilemann. 2019. Synthetic and genetic dimers as quantification ruler for single-molecule counting with PALM. Mol Biol Cell 30:1369-1376.
41. Hartwich, T. M., F. V. Subach, L. Cooley, V. V. Verkhusha, and J. Bewersdorf. 2013. Determination of two-photon photoactivation rates of fluorescent proteins. Phys Chem Chem Phys 15:14868-14872.
42. Subach, F. V., V. N. Malashkevich, W. D. Zencheck, H. Xiao, G. S. Filonov, S. C. Almo, and V. V. Verkhusha. 2009. Photoactivation mechanism of PAmCherry based on crystal structures of the protein in the dark and fluorescent states. Proc Natl Acad Sci U S A 106:21097-21102.
43. De Zitter, E., D. Thedie, V. Monkemoller, S. Hugelier, J. Beaudouin, V. Adam, M. Byrdin, L. Van Meervelt, P. Dedecker, and D. Bourgeois. 2019. Mechanistic investigation of mEos4b reveals a strategy to reduce track interruptions in sptPALM. Nat Methods 16:707-710.

Figures

Figure 1

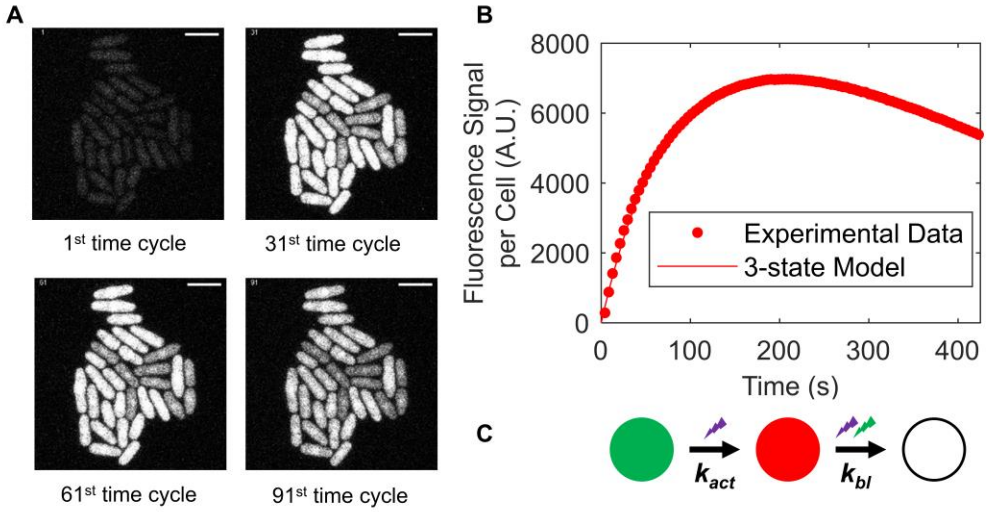

Figure 1: Photoconversion and photobleaching of mEos3.2. (A) Time series of fluorescence micrographs of a field of *S. pombe* cells expressing cytoplasmic mEos3.2 at the 1st, 31st, 61st, and 91st time cycles. At each of the 100 cycles, a point-scanning confocal microscope illuminated the cells simultaneously at both 405 nm and 561 nm, 19-slices in a Z stack were imaged with a total exposure time of 4.23 s and sum-projected with the same contrast. Scale bar = 10 µm. **(B)** Time course of the fluorescence signal per cell at 566-719 nm (after autofluorescence subtraction). Fitting Eq. 7 of the 3-state model in panel C (line) to the data (dots) gave a photoconversion rate constant (k_{act}) of 1.2 x 10^{-2} s^{-1} (95% CI: 1.16 -1.24 x 10^{-2}) and a photobleaching rate constant (k_{bl}) of 1.6 x 10^{-3} s^{-1} (95% CI: 1.5-1.7 x10^{-3}). **(C)** Three state model for mEos3.2 photoconversion and bleaching. Illumination at 405 nm photoconverts mature mEos3.2 molecules from the green (G) state to the red (R) state with a photoconversion rate constant of k_{act}. Illumination at both wavelengths photobleaches red mEos3.2 molecules with a rate constant of k_{bl}.

Figure 2

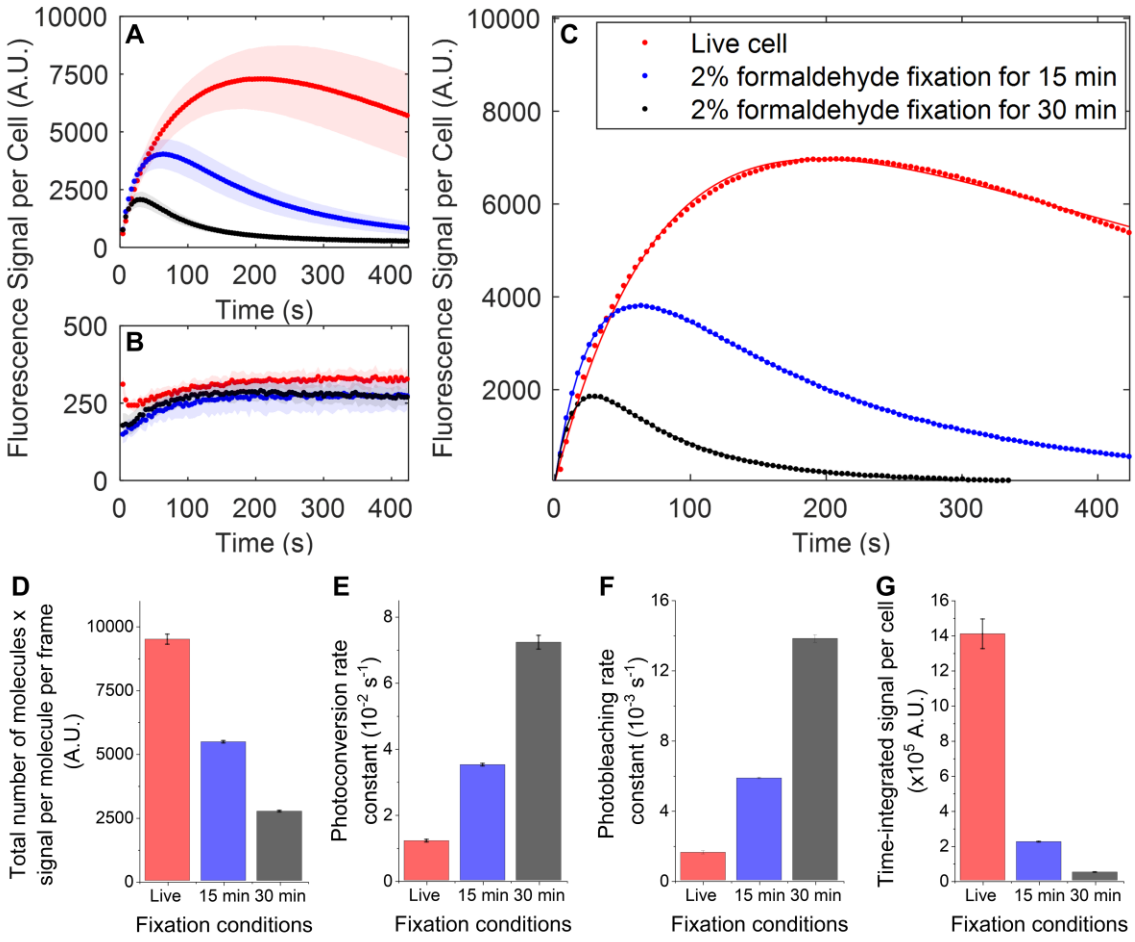

Figure 2: Effects of formaldehyde fixation on the fluorescence signal of mEos3.2 and rate constants for photoconversion and photobleaching. (A) Time courses of the fluorescence signal per *S. pombe* cell expressing cytoplasmic mEos3.2 illuminated at 405 nm (22 µW) and 561 nm (15 µW) by point-scanning confocal microscopy under 3 conditions: live cells (red dots) or cells fixed with 2% formaldehyde for 15 min (blue dots) or 30 min (black dots) in EMM5S medium and imaged in EMM5S. Nine fields of view (FOV) of 85 µm x 85 µm were taken over time for each condition. Plots are weighted mean (dots) and standard deviations (shaded area) of the fluorescence signal per cell. **(B)** Time courses of the total autofluorescence signal per wild type *S. pombe* cell under the same conditions as in panel A. Four FOVs of 85 µm x 85 µm over time were taken for each condition. Plots show weighted mean (dots) and standard deviations (shaded area) of the fluorescence signal per cell. **(C)** Time courses of the mEos3.2 fluorescence

signal per cell at 566-719 nm after autofluorescence subtraction. Eq. 7 of the 3-state model was fit to the experimental data (dots). The lines are theoretical curves using the parameters that best fit the data. **(D-G)** Comparison of parameters of live cells and cells fixed for 15 or 30 min. The error bars are 95% confidence intervals of the parameters (Table S1). **(D)** The product of total number of molecules per cell and signal of a R-state mEos3.2 molecule per frame (M_n x ε_f) from the fit. **(E)** Photoconversion rate constant (k_{act}) from the fit. **(F)** Photobleaching rate constant (k_{bl}) from the fit. **(G)** Time-integrated signal per cell ($\overline{R_s}$) calculated using Eq. 8.

Figure 3

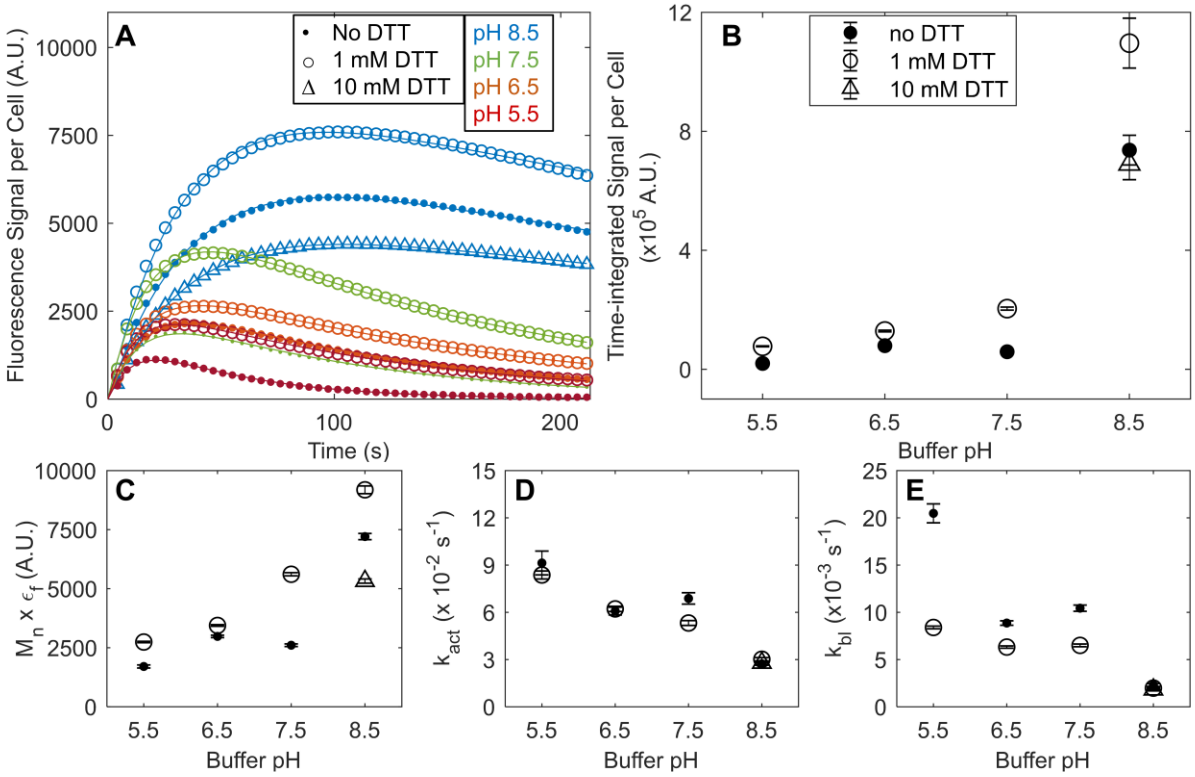

Figure 3: Effects of pH and DTT on the fluorescence signal and rate constants for photoconversion and photobleaching of mEos3.2 in fixed *S. pombe* cells. (A) Time courses of the fluorescence signal per cell expressing cytoplasmic mEos3.2 (after autofluorescence subtraction). The cells were fixed with 2% formaldehyde for 30 min and illuminated at 405 nm (22 µW) and 561 nm (15 µW) by point-scanning confocal microscope under 9 different buffer conditions: (red dot) 50 mM MES (pH 5.5); (red circle) 50 mM MES (pH 5.5) with 1 mM DTT; (orange dot) 50 mM MES (pH 6.5); (orange circle) 50 mM MES (pH 6.5) with 1 mM DTT; (green dot) 50 mM Tris-HCl (pH 7.5); (green circle) 50 mM Tris-HCl (pH 7.5) with 1 mM DTT; (blue dot) 50 mM Tris-HCl (pH 8.5); (blue circle) 50 mM Tris-HCl (pH 8.5) with 1 mM DTT: (blue triangle) 50 mM Tris-HCl (pH 8.5) with 10 mM DTT. The continuous lines are best fits of Eq. 7 of the 3-state model to the time courses of the fluorescence signal per cell. Fig. S4 reports the raw data. **(B-E)** Dependence of the parameters on pH and DTT. The error bars are 95% confidence intervals for the parameters (Table S2). **(B)** Time-integrated signal per cell ($\overline{R_s}$) calculated using Eq. 8. **(C)** The product of total number of molecules per cell and the signal of a

R-state mEos3.2 molecule per frame (M_n x ε_f) from the fit. **(D)** Photoconversion rate constant (k_{act}) from the fit. **(E)** Photobleaching rate constant (k_{bl}) from the fit.

Figure 4

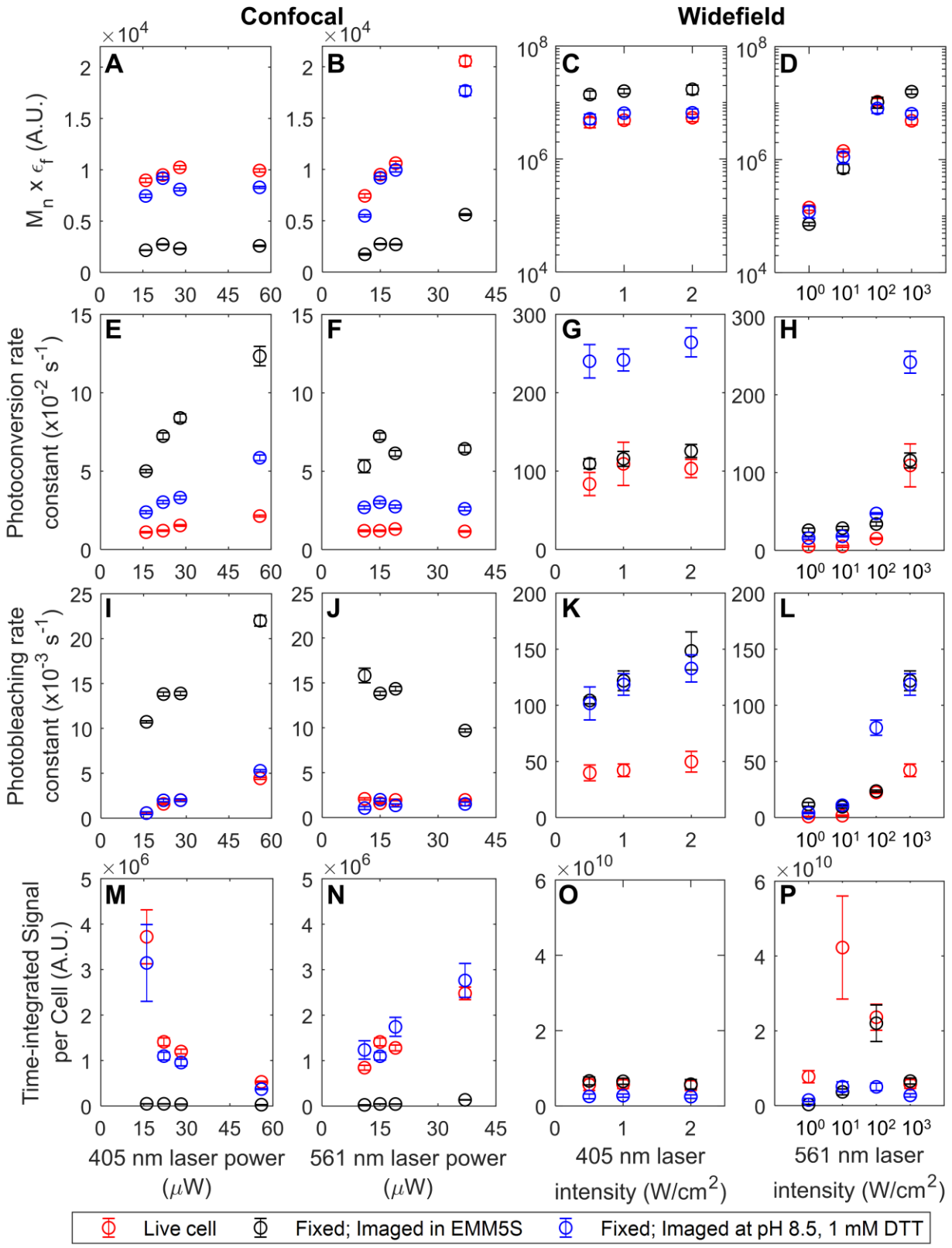

Figure 4: The effects of 405-nm and 561-nm laser intensities on the fluorescence signal and rate constants for photoconversion and photobleaching of mEos3.2 in live and fixed *S. pombe* cells. Cells expressing cytoplasmic mEos3.2 were imaged live (red circles) or fixed with 2% formaldehyde for 30 min in EMMS5 medium and mounted in EMM5S medium (black circles) or 50 mM Tris-HCl (pH 8.5) with 1 mM DTT (blue circles). Cells were imaged with 7 different laser intensities by confocal microscope and 6 different laser intensities by epi-fluorescence microscope. For confocal imaging, 561 nm laser power was set at 15 μW for panels A, E, I, M; 405 nm laser power was set at 22 μW for panels B, F, J, N. Four FOVs were taken for each condition with cells expressing mEos3.2. Two FOVs were taken for each condition with wild type cells. For epi-fluorescence imaging, 561 nm laser intensity was set at 1 kW/cm^2 for panels C, G, K, O; 405 nm laser intensity was set at 1 W/cm^2 for panels D, H, L, P. Eight to ten FOVs were taken for each condition with cells expressing mEos3.2. Three or four FOVs were taken for each condition with wild type cells. Eq. 7 of the 3-state model was fit to the time courses of fluorescence signal to determine the parameters giving the best fit: **(A-D)** The product of total number of molecules per cell and the signal of a R-state mEos3.2 molecule per frame (M_n x ε_f); **(E-H)** photoconversion rate constant (k_{act}); and **(I-L)** photobleaching rate constant (k_{bl}) (Table S3, S4). **(M-P)** Time-integrated signal per cell ($\overline{R_s}$) calculated using Eq. 8 (Table S3, S4). The error bars in the left 2 columns are 95% confidence intervals of the fit. The error bars in the right 2 columns are the weighted standard deviations among different FOVs. Fig. S5 and S6 report the raw data.

Figure 5

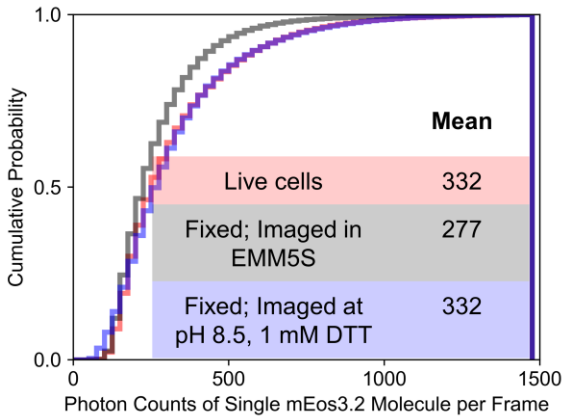

Figure 5: The effect of fixation and imaging buffer on photon counts from mEos3.2 by single molecule localization microscopy (SMLM). SMLM imaging of cytoplasmic mEos3.2 in *S. pombe* cells with continuous illumination at 405 nm (1 W/cm^2) and 561 nm (1 kW/cm^2) under 3 conditions: live cells (red), cells fixed with 2% formaldehyde in EMM5S medium for 30 min and mounted in EMM5S synthetic medium (black) or mounted in 50 mM Tris-HCl (pH 8.5) with 1 mM DTT) (blue). Four FOVs of 40 µm x 40 µm were taken over time at 50 fps for 15,000 frames for each condition. All emission bursts between frame 5,000 and 10,000 were localized to measure the photon counts from single red mEos3.2 molecules in each 20-ms frame, when the mEos3.2 molecules were sparse enough for Gaussian center fitting. The curves show the cumulative probability distribution of the photon counts of single mEos3.2 molecules in each 20-ms frame under all three conditions. Insert: The table reports the mean number of photons emitted by single mEos3.2 molecules in each 20-ms frame under the three conditions. About 2 – 5 x 10^5 emission bursts were recorded for the histogram.

Figure 6

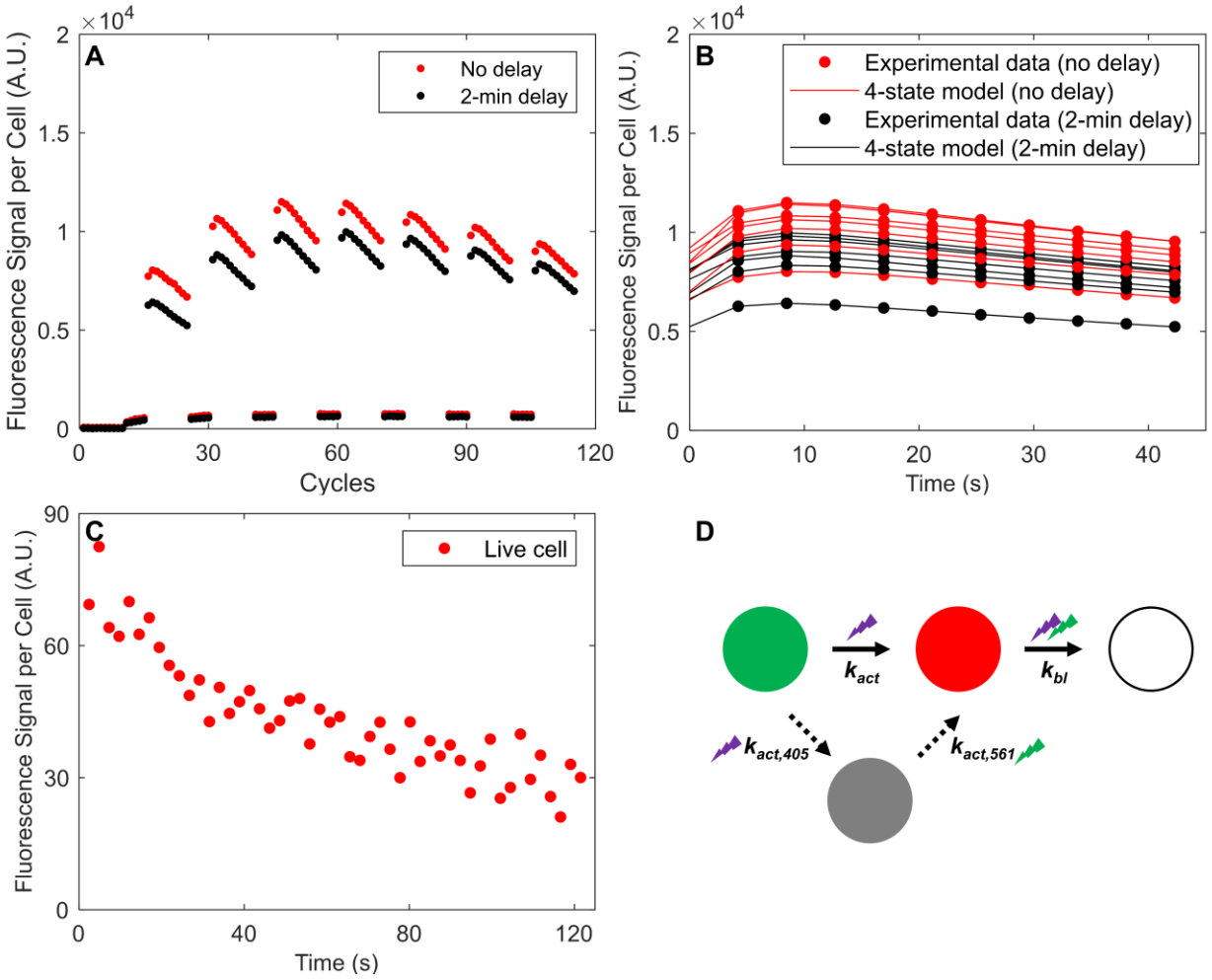

Figure 6: A second pathway to convert mEos3.2 from the green state to the red state requires both 405-nm and 561-nm illumination. (A) Time courses of the fluorescence signal per live *S. pombe* cell expressing mEos3.2 and subjected to alternating illumination by point-scanning confocal microscopy at 561 nm (37 µW) for 10 cycles followed by illumination at 405 nm (56 µW) for 5 cycles. Illumination at 561 nm increased the fluorescence signal beyond the start of the 561-nm illumination period after each period of 405-nm illumination. The red dots are data collected from live cells with no delay between the periods of illumination at 405 nm and 561 nm, while the black dots are data collected from live cells with a 2-min break after each period of 405-nm illumination before the following period of 561-nm illumination. **(B)** Comparisons of the time courses of the fluorescence signals during 7 periods with 10 cycles of 561-nm illumination (not including the first 561-nm illumination period before any 405-nm irradiation) from panel A. Eq. 14 of the 4-state model in panel D (lines) was fit to these time

courses (dots) to determine rate constants giving the best fit. The mean activation rate constant ($k_{act,561}$) from the I-state to the R-state is 0.27 s^{-1} (SD: 0.03) for the experiment with no delay between the 405-nm and 561-nm illumination cycle (red), and 0.28 s^{-1} (SD: 0.03) for the experiment with 2-min breaks (black). **(C)** Time course of the fluorescence signal per cell expressing mEos3.2 and illuminated only at 561 nm (37 µW). **(D)** Four-state model for mEos3.2 photoconversion and bleaching. Illumination at 405 nm photoconverts mature mEos3.2 molecules from the G-state to either the R-state with a photoconversion rate constant of k_{act} or to the I-state with a photoconversion rate constant of $k_{act,405}$. Irradiation at 561 nm photoconverts I-state mEos3.2 molecules to the R-state with a rate constant of $k_{act,561}$. Illumination at both wavelengths photobleaches red mEos3.2 molecules with a rate constant of k_{bl}.

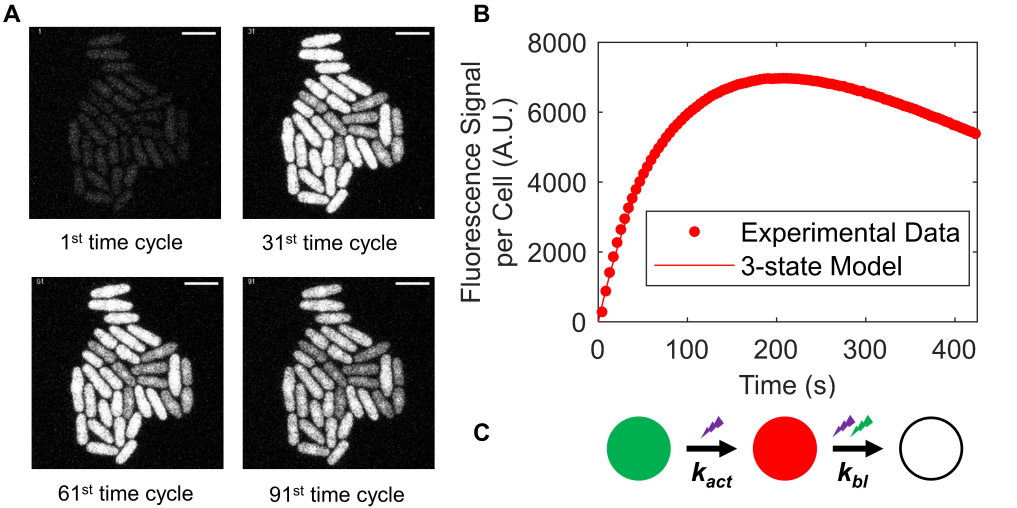
A
1st time cycle
31st time cycle
61st time cycle
91st time cycle
B
Fluorescence Signal per Cell (A.U.)
8000
6000
4000
2000
0
0
100
200
300
400
Time (s)
Experimental Data
3-state Model
C
k_{act}
k_{bl}

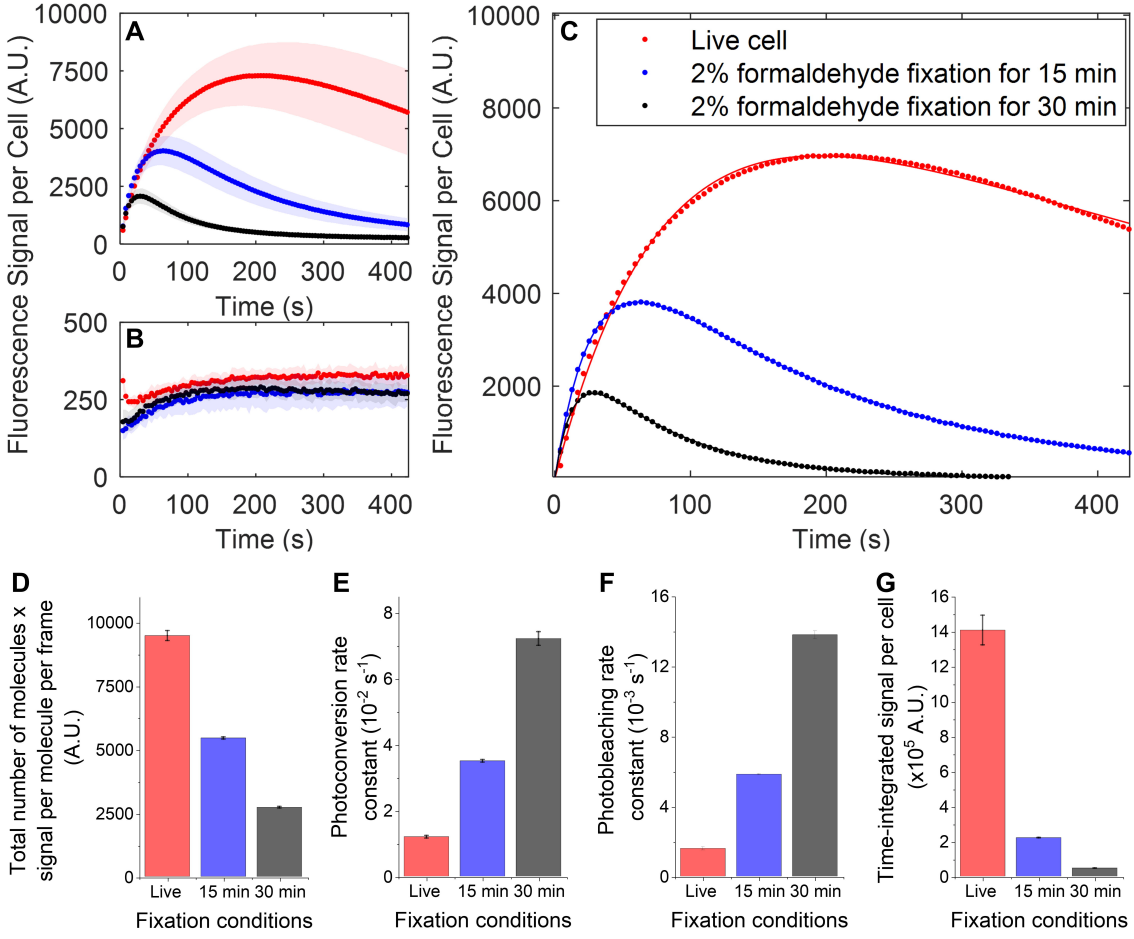
A
B
C
D
E
F
G
Fluorescence Signal per Cell (A.U.)
Time (s)
Live cell
2% formaldehyde fixation for 15 min
2% formaldehyde fixation for 30 min
Total number of molecules x signal per molecule per frame (A.U.)
Photoconversion rate constant (10-2 s-1)
Photobleaching rate constant (10-3 s-1)
Time-integrated signal per cell (x105 A.U.)
Live
15 min
30 min
Fixation conditions

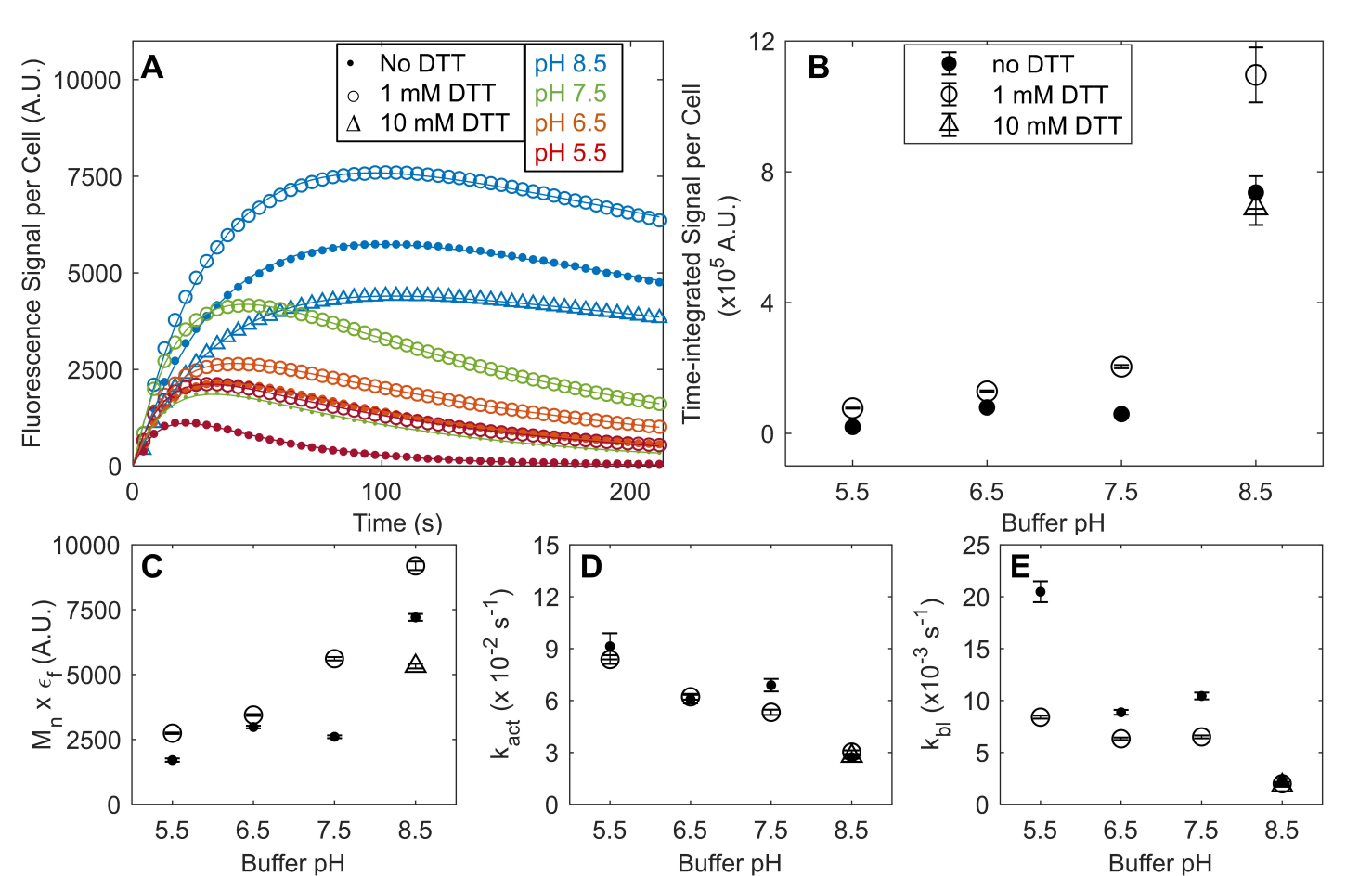
A
No DTT
1 mM DTT
10 mM DTT
pH 8.5
pH 7.5
pH 6.5
pH 5.5
Fluorescence Signal per Cell (A.U.)
Time (s)
B
no DTT
1 mM DTT
10 mM DTT
Time-integrated Signal per Cell (x10^5 A.U.)
Buffer pH
C
M_n x ε_f (A.U.)
Buffer pH
D
k_act (x 10^-2 s^-1)
Buffer pH
E
k_bl (x10^-3 s^-1)
Buffer pH

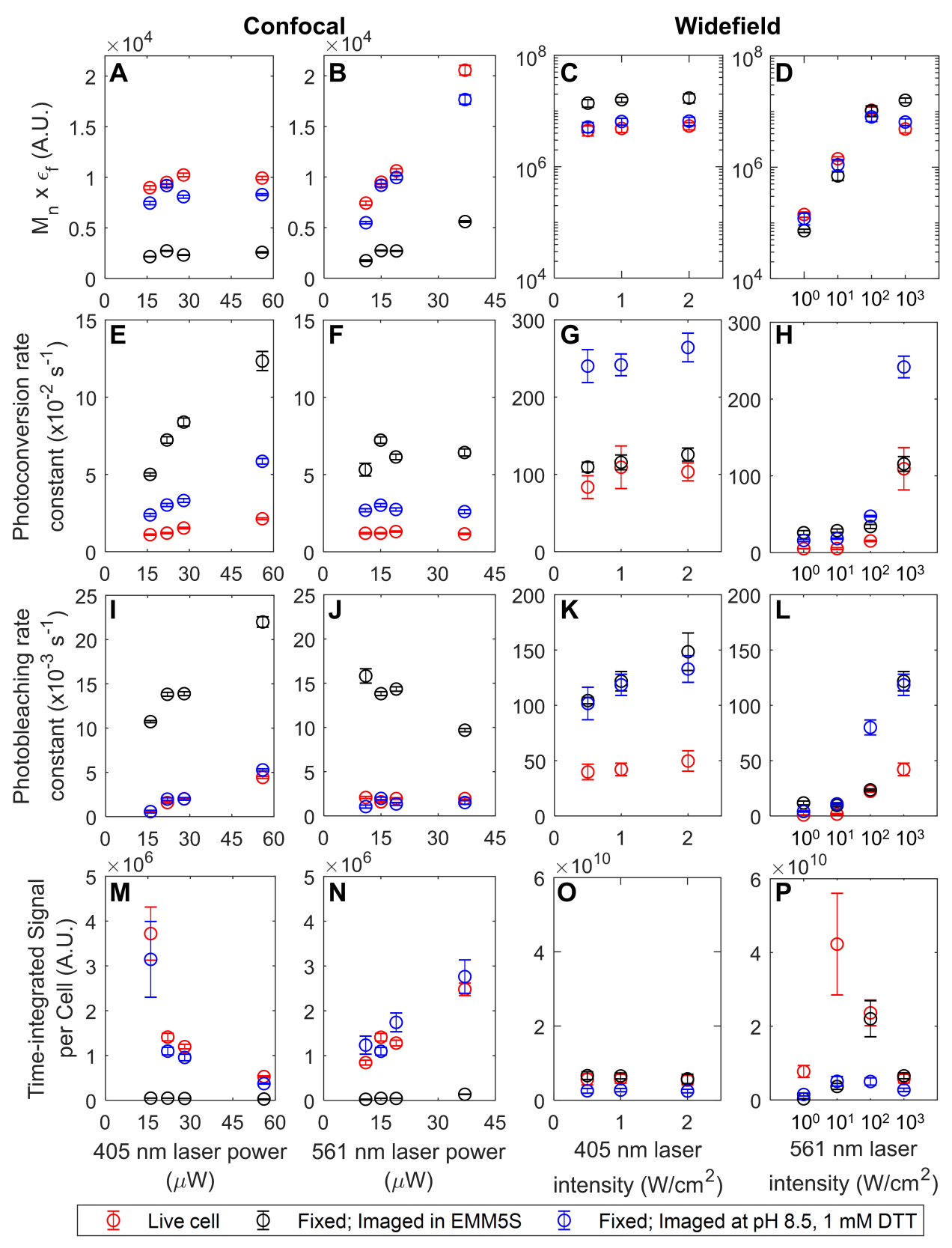
Confocal
Widefield
A
B
C
D
E
F
G
H
I
J
K
L
M
N
O
P
$M_n \times \epsilon_f$ (A.U.)
Photoconversion rate constant (x10^{-2} s^{-1})
Photobleaching rate constant (x10^{-3} s^{-1})
Time-integrated Signal per Cell (A.U.)
405 nm laser power (μW)
561 nm laser power (μW)
405 nm laser intensity (W/cm^2)
561 nm laser intensity (W/cm^2)
Live cell
Fixed; Imaged in EMM5S
Fixed; Imaged at pH 8.5, 1 mM DTT

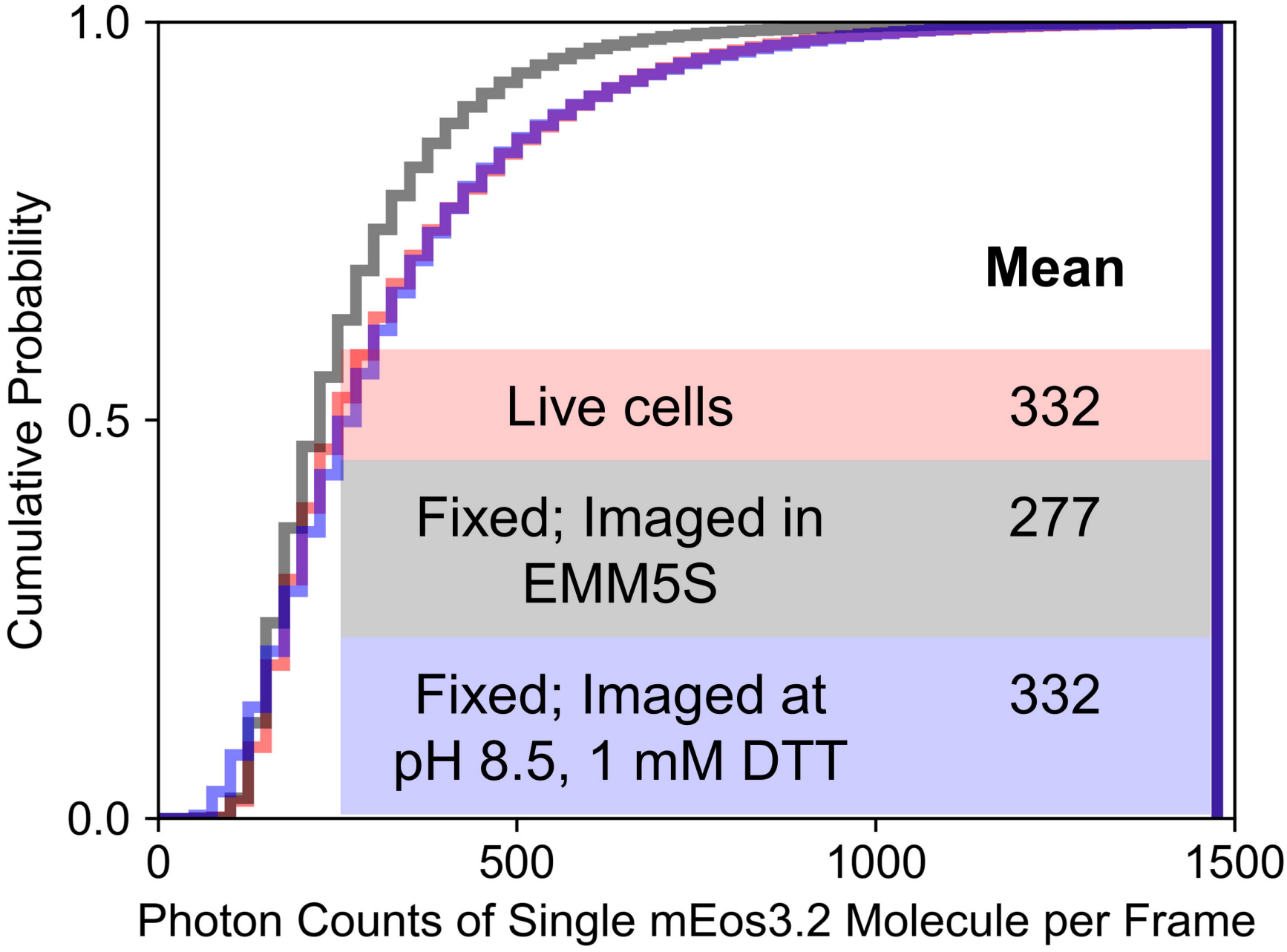
1.0
0.5
0.0
Cumulative Probability
0
500
1000
1500
Photon Counts of Single mEos3.2 Molecule per Frame
Mean
Live cells
332
Fixed; Imaged in EMM5S
277
Fixed; Imaged at pH 8.5, 1 mM DTT
332

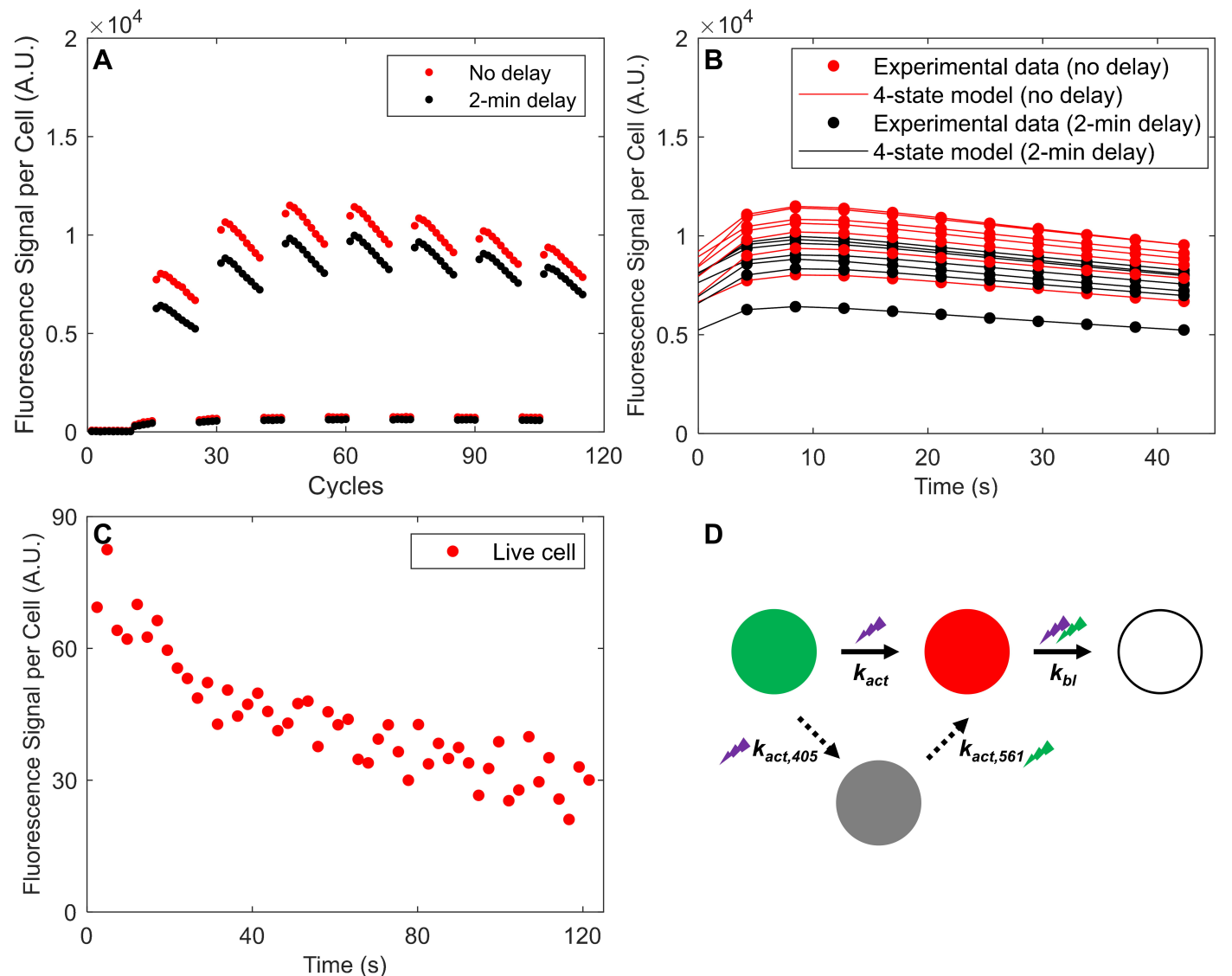
A
No delay
2-min delay
Fluorescence Signal per Cell (A.U.)
Cycles
B
Experimental data (no delay)
4-state model (no delay)
Experimental data (2-min delay)
4-state model (2-min delay)
Fluorescence Signal per Cell (A.U.)
Time (s)
C
Live cell
Fluorescence Signal per Cell (A.U.)
Time (s)
D
k_{act}
k_{bl}
$k_{act,405}$
$k_{act,561}$